

Aerodynamics and Aeroacoustics of Sail Masts

Ali Ghadiani

**Supervisors: Gabriele Bellani, University of Bologna
Huadong Yao, Chalmers university of technology**

A thesis presented for the degree of
SECOND CYCLE MASTER'S DEGREE in INGENERIA
AEROSPAZIALE/AEROSPACE ENGINEERING
Class LM-20

SCHOOL OF ENGINEERING AND ARCHITECTURE
ALMA MATER STUDIORUM UNIVERSITA DI
BOLOGNA
ITALY

December 2019

Abstract

In this thesis, the turbulent flow induced by sail masts is simulated using compressible $k - \omega$ SST detached eddy simulation(DES). The mast is investigated in two different yaw angles at $\psi = 0^\circ$ and $\psi = 90^\circ$ and predetermined condition is $V = 20 \frac{m}{s}$ to find the main broadband and tonal noise sources. And then the same cases are compared to simple shape of mast without internal cavities. A purpose of this work is to investigate whether the cases generate tonal noise when winds past the sail mast. Another objective is to study aerodynamic parameters around the four cases. The influence of the mast tips are assessed and the Sound Pressure Levels(SPL) that are gotten from pressure fluctuations are shown at the end to find the tonal noise and show the study cases with cavity inside make much more noise than simplified sail mast. By looking at the peaks in the sound pressure level(SPL) the tonal noise at specific frequencies can be found.

The commercial software STAR-CCM+ was used for all three parts pre-processing, running simulations, and post-processing to understand the noise generation and aerodynamic features.

Preface

This report presents the work done for master thesis and Detached Eddy Simulation (DES) has been performed on a sail mast to compare with simplified sail mast in two different yaw angles. The work has been carried out from September 2018 to February 2019 at the Department of Mechanics and Maritime Sciences at Chalmers University of Technology, Sweden, with Ali Ghadiani as student and Hua-Dong Yao as supervisor. The scope of work has been to study the physics of the study cases and apply STAR-CCM+ and Detached Eddy Simulations to simulate the flow. A three dimensional Computational Fluid Dynamics analysis has been carried out for sail mast and simplified sail mast geometry with Reynolds number equal to $Re = 3.636 \times 10^5$.

The main goal was to run analyses for sail mast and simplified sail mast in two different positions and compare the results, as well as understanding the physics involved in the cases. Learning to use the software system STAR-CCM+ for Computational Fluid Dynamic (CFD) and Computational aero-acoustic analyses played the most important role in this project. As we could find out from the thesis results this work has been very rewarding because this thesis topic is new and this time some impressive results have been found.

During the project much time was spent on the pre-processing part of the analyses and running the simulations. The simulations were run in Swedish National Infrastructure for Computing (SNIC) which could help me a lot to find my mistakes in short time. In addition having experience to work with cluster to run fluid dynamic simulation was another advantage that i could gain during my master thesis at Chalmers university of technology.

Dedication

I dedicate this thesis to my family for nursing me with affections and love and their dedicated partnership for success in my life.

Acknowledgements

Several persons have been engaged and helped me during the master thesis work. First of all i would like to thank my supervisor, Hua-Dong Yao for giving me this chance to work on this new and challenging master thesis. His guidance and support that he did during the thesis in Chalmers University of Technology. And i would like to mention Hamidreza Abedi, Guglielmo Minelli and Bercelay Niebles Atencio who helped me a lot when I was doing my master thesis and having always open door and answering all my questions to handle my work well. The Swedish National Infrastructure for Computing (SNIC) should be mentioned here since it provides computational resources for this work.

At the end i want to tanks my supervisor Gabriele Bellani at university of Bologna for his exact advice and great moral support during my master thesis.

Contents

1	introduction	11
2	Background	12
2.1	Background	12
2.1.1	Sail Mast model	13
3	Theory	14
3.1	Fluid mechanics	14
3.1.1	Equations of Motion	14
3.1.2	Fundamental Definitions	15
3.2	Turbulent flow	18
3.3	Acoustic theory	19
3.4	Computational Method theory	22
3.4.1	Computational Fluid Dynamics (CFD) and Computational Aeroacoustics (CAA)	22
3.4.2	Ffowcs Williams Hawkings (FWH) acoustic analogy	23
3.4.3	Prediction of noise	24
4	Computational setting	26
4.1	Pre-processing	26
4.1.1	CFD domain and physics setup	26
4.1.2	Mesh generation method	28
4.1.3	FWH permeable surface and far-field microphones	31
4.2	Post-processing	31
4.2.1	Fast Fourier transform and sound pressure level	32
4.2.2	Plotting results	33
5	Results	34
5.1	Flow characteristics	34
5.1.1	Velocity	34
5.1.2	Pressure	37
5.1.3	Contour plots of vorticity	38
5.1.4	Visualization of flow structures	42
5.1.5	Velocity profile and force coefficients	43
5.2	Sound sources	46
5.2.1	Far-field noise	48

6 Conclusion	51
6.1 Final discussion	51
6.2 Future work	52
A Appendix	53
A.1 Streamline	53
A.2 Variance	53
A.3 Overall sound pressure level	54

List of Figures

2.1	Sail mast of a moored boat	12
2.2	Spanwise deirection of the sail mast	13
2.3	Geometry of computational domain	13
3.1	The history of the drag and lift coefficients obtained for the simplified sail mast in 1 second physical time to be compared	17
3.2	Turbulent flow on downstream of simplified sail mast at $\psi = 0^\circ$ colored by pressure in range of $1.009 \times 10^5(\text{Pa})$ and $1.0157 \times 10^5(\text{Pa})$.	19
4.1	computational domain and sail mast dimensions which are shown by top and side view	27
4.2	Prism layers located around sail mast's tips	28
4.3	Mesh design of whole computational domain with the sail mast at $\psi = 0^\circ$	30
4.4	Refinement part of mesh design	30
4.5	Location of Receivers around the computational domain by radius of $10m$	31
5.1	Velocity contour plots for $\psi = 0^\circ$ in range of $0\frac{m}{s}$ to $40\frac{m}{s}$ shown by plane section at $y = 0$ and $x = 0$	35
5.2	Velocity magnitude contour plots for $\psi = 90^\circ$ in range of $0\frac{m}{s}$ to $40\frac{m}{s}$ shown by plane section at $y = 0$ and $x = 0$	35
5.3	Mean velocity magnitude at $\psi = 0^\circ$ in range of $0\frac{m}{s}$ to $40\frac{m}{s}$ shown by plane section at $y=0$ and $x=0$	36
5.4	Power Spectral Density(PSD) of velocity in all three probes and compare them to each other which is plotted in different frequencies between $0(Hz)$ to $4500(Hz)$	36
5.5	Power Spectral Density(PSD) of velocity in tip probes and compare them to each other which is plotted in different frequencies between $0(Hz)$ to $4500(Hz)$	37
5.6	Pressure contour plots for $\psi = 0^\circ$ in range of $1.0051 \times 10^5(\text{Pa})$ to $1.0172 \times 10^5(\text{Pa})$ shown by plane section at $y=0$ and $x=0$	38
5.7	Pressure contour plots for $\psi = 90^\circ$ in range of $1.0051 \times 10^5(\text{Pa})$ to $1.0172 \times 10^5(\text{Pa})$ shown by plane section at $y=0$ and $x=0$	38
5.8	Vorticity magnitude contour plots at $\psi = 0^\circ$ in range of $0s^{-1}$ to $1000s^{-1}$ shown by plane section at $y=0$ and $x=0$	39
5.9	Vorticity magnitude contour plots at $\psi = 90^\circ$ in range of $0s^{-1}$ to $1000s^{-1}$ shown by plane section at $y=0$ and $x=0$	40

5.10	Top view of probe's locations around the sail mast and simplified mast to measure pressure and velocity	41
5.11	Comparison of static pressure on tip probes in among all four cases which is plotted in different frequencies between $0(Hz)$ to $4500(Hz)$.	41
5.12	Comparison of static pressure on left side probes among all four cases which is plotted in different frequencies between $0(Hz)$ to $4000(Hz)$.	42
5.13	Comparison of static pressure on right side probes among all four cases which is plotted in different frequencies between $0(Hz)$ to $4000(Hz)$	42
5.14	Flow structures colored by pressure at $\psi = 0^\circ$	43
5.15	Flow structures colored by pressure at $\psi = 90^\circ$	43
5.16	Velocity and pressure profiles for $\psi = 0^\circ$ along z direction	44
5.17	Velocity and pressure profiles for $\psi = 90^\circ$ along z direction	44
5.18	Comparison of flow structure affected by cavity and bluff body on down stream colored by pressure in range of 1.009×10^5 and 1.0157×10^5 ,case studies at $\psi = 0^\circ$	46
5.19	Comparison of flow structure affected by cavity and bluff body on down stream colored by pressure in range of 1.009×10^5 and 1.0157×10^5 ,case studies at $\psi = 90^\circ$	47
5.20	Pascal Second graph of all 36 Receivers located around computational domain	48
5.21	Comparison of Sound Pressure Level(SPL) graph in all four cases which are changed by different frequencies between $30(Hz)$ to $5000(Hz)$ 50	
A.1	Streamline colored by velocity in streamwise direction at $\psi = 0^\circ$. . .	53
A.2	Streamline colored by velocity in stream wise direction at $\psi = 90^\circ$. .	53

List of Tables

2.1	Flow properties	13
3.1	Air Density and Viscosity	15
3.2	Speed of sound	21
4.1	Case dimensions	27
4.2	Mesh characteristics	29
5.1	Drag and lift coefficients	44

Chapter 1

introduction

The sail mast that is considered in this thesis is a simplified shape of industrial sail mast. The results are used to indicate the basic flow mechanisms near sail masts and far-field noise determination. This study aims to investigate the noise sources of the sail mast and show the aerodynamic features around all four study cases. The advanced CFD method, compressible detached eddy simulation (DES), will be explored for its suitability in the development of this case[25] and far field noise is predicted by Ffowcs William and Hawkings (FW-H) acoustic analogy.

The features of pressure fluctuations on the sail mast which could be interesting will be shown and the numerical methodology used in the flow computation is described in Computational Theory. The numerical settings specified for the computation are provided in Computation Settings. The mesh study is reported in Mesh Design section. And this work can be a great connection between aerodynamic and aero-acoustic field to see how they affect on each other.

Chapter 2

Background

2.1 Background



Figure 2.1: Sail mast of a moored boat

There are things that sailors can not change like wind and waves, but they can choose some equipment with higher quality and look for a company which cares about the detail of their products.

Sail masts are usually designed by aluminum and carbon fiber. A general sail mast shape is like an elliptical shape with an integral luff groove at its trailing edge. In this thesis the noise generation and aerodynamics of a sail mast is going to be studied. It can be lead to improvement of sail mast's shape in future and it can be

strong fundamental work about aero-acoustic field which connects aerodynamic and acoustic areas to each other.

If a sail boat is considered here, the boat can be located in different positions the directions of winds can be changed. The cases at yaw angles of $\psi = 0^\circ$ and $\psi = 90^\circ$ are considered in this study which are specific positions of sail mast.

2.1.1 Sail Mast model

The flow simulation is conducted for a part of the sail mast that the spanwise dimension of both masts is 500 mm , cross section of both shapes is $150\text{ mm} \times 270\text{ mm}$ and they are simulated at two yaw angles $\psi = 0^\circ$ and $\psi = 90^\circ$. The free steam characteristics are $u_\infty = 20 \frac{\text{m}}{\text{s}} = 72 \frac{\text{km}}{\text{h}}$, $p_\infty = 101325\text{ Pa}$, $T_\infty = 288\text{ K}$, $Ma = 0.058$ and $Re = 3.636 \times 10^5$ and wind comes from Z direction. As noise generated by turbulence, $3D$ computations are performed by Detached Eddy Simulation (DES). So some challenges like numerical errors, Divergence problem and mesh generation could be happen along the simulation process.

The software system STAR-CCM+ will be used and master student shall demonstrate the use of the program on this application. Furthermore some regions are extremely important like wake region and near the sail mast tips that we need to analyze them very carefully.

$u_\infty [\frac{\text{m}}{\text{s}}]$	$T [\text{K}]$	$P_\infty [\text{pa}]$	$\rho [\frac{\text{kg}}{\text{m}^3}]$	$\mu [10^{-5} \frac{\text{kg}}{\text{m.s}}]$	$k [10^{-3} \frac{\text{W}}{\text{m.K}}]$	$C_p [\frac{\text{J}}{\text{kg.K}}]$	Pr
20	288	101325	1.225	1.796	25.24	1006	0.7156

Table 2.1: Flow properties



Figure 2.2: Spanwise deirection of the sail mast



Figure 2.3: Geometry of computational domain

Chapter 3

Theory

3.1 Fluid mechanics

3.1.1 Equations of Motion

When velocity and two thermodynamic variables are specified the fluid is defined by time and location. So some equations are needed for determination of fluid motion and these equations are statements of the conservation of mass,energy and momentum.

Continuity Equation

Mass conservation needs the rate of increase of the mass in control volume to be the same as the net influx that is convected across the boundaries of control volume. Furthermore velocity and density have to satisfy the equation of continuity. In addition if our study case is incompressible fluid $divv$ will be zero in our calculation but in the thesis we are facing to compressible flow.

$$\left\{ \begin{array}{l} \frac{\partial \rho}{\partial t} + div(\rho v) = 0 \\ \frac{1}{\rho} \frac{D\rho}{Dt} + divv = 0 \\ divv = \rho \frac{D}{Dt} \left(\frac{1}{\rho} \right) \end{array} \right\}$$

Momentum Equation

Momentum equation shows how momentum of fluid particle change in term of the pressure p,the viscous,and body forces F per unit volume. This equation is suitable approximation in air for calculating frictional drag around the study cases for which the frictional forces are defined in terms of the shear coefficient of viscosity η ,which we consider it to be constant.

$$\rho \frac{Dv}{Dt} = -\nabla p + \eta(\nabla^2 v + \frac{1}{3}\nabla(divv)) + F \quad (3.1)$$

Energy Equation

This equation is used in its full generality in problems where energy is transferred by heat conduction,where frictional dissipation of sound is occurring,or when sound

Parameter	$\rho, \frac{kg}{m^3}$	$\eta, \frac{kg}{m.s}$	$\mu, \frac{m^2}{s}$
Air	1.23	1.764×10^{-5}	1.433×10^{-5}

Table 3.1: Air Density and Viscosity

is being generated by combustion and other heat sources.[13] In our case we consider the specific entropy s of the fluid is uniform and constant throughout the fluid. We assume that pressure and density are related by this equation:

$$p = p(\rho, s), s = constant \quad (3.2)$$

This equation can be used for undisturbed and unsteady components of the flow. For ideal gas we can write that which γ is ration of specific heats

$$p = constant \times \rho^\gamma \quad (3.3)$$

3.1.2 Fundamental Definitions

Some definitions should be presented here to show the fundamental conditions for running the simulations. In the following part aerodynamics and aero-acoustic definitions which are related to the thesis are presented.

Compressible flow

Numerical simulation can be done for two kind of cases compressible and incompressible flow. In this case the flow is compressible so the density is not constant and is changing by time. The flow undergoes a notable variant in density with trending pressure in time and space. By considering velocity is a constant value during the simulation we can calculate the Mach number by the fraction of flow velocity over velocity of sound in air: $V = 20 \frac{m}{s}, c_0 = 340 \frac{m}{s}$

$$Ma = \frac{V}{c_0} = \frac{20}{340} = 0.058 \quad (3.4)$$

Reynolds number and flow regime

It is important to keep the Reynolds number (Re) constant when we investigate the different cases because it determines the probability of the flow being turbulent or laminar. The Reynolds formula is shown here: $\rho = 1.225 \frac{kg}{m^3}, V = 20 \frac{m}{s}, L = 0.27m, \mu = 1.796 \times 10^{-5} \frac{kg}{m.s}$

$$Re = \frac{\rho V L}{\mu} = \frac{V L}{\nu} = \frac{1.225 \times 20 \times 0.27}{1.796 \times 10^{-5}} = 3.636 \times 10^5 \quad (3.5)$$

As we can see the equation we need to care about each parameter to keep the Re number constant, like velocity of fluid (V), length of the sail mast (L), Density (ρ), Kinematic viscosity (ν) and Dynamic viscosity (μ). If we increase Re number the length of vortices will be increased and when the Reynolds number increased more the wake region become unstable and vortices are shed at the both side of sail mast, then we have vortex street. By increasing Reynolds number (Re) turbulent occur in the wake region and we can see the vortices are shed in span wise direction.

Vortex shedding

When the Reynolds number (Re) number passes a limit boundary layer over the sail mast will separate due to the adverse pressure gradient and its pressure gradient increases because of divergence environment of the flow at the downstream of the sail mast. The boundary layer along the sail mast contains a significant amount of vorticity and the vorticity will continue to the shear layer downstream of the sail mast and cause roll into the vortex. The vorticity vector $\omega = \nabla \times V$ is a measure of rotational effects and it is equal to local angular velocity of a fluid. If we want to talk about vortex shedding this topic can be started by size of this item. When the larger vortex becomes strong enough it goes to the opposite vortex across the wake.

Strouhal number

To find the Strouhal number (St), the vortex shedding period can be found from oscillating pressure or velocities in probes that I have put near the sail mast and around the cavity. By normalizing the frequency we have Strouhal number and it can be found in different frequencies which are interesting for us like at peak of the pressure fluctuation. Strouhal number can be found by multiplication between frequency and diameter of the model over velocity of fluid.

$$St = \frac{fD}{U}, f = \frac{1}{T} \quad (3.6)$$

This value is strongly related to Re number and the level of frequency of St number is related to the scale of instability. If we have large instability we have low frequency St number that is not related to the Re number and high frequency St is caused by small scale instabilities, also when the vortices interact each other the vortex shedding frequency will increase. Usually Strouhal number at low frequency is equal to 0.2.

Aerodynamic forces

When we are talking about aerodynamic of sail mast different forces are mentioned which are lift and drag. The drag force is a combine of skin friction and pressure coefficient, this is also applied to lift coefficient.

$$F_D = F_p + F_F \quad (3.7)$$

Drag coefficient and lift coefficient definition are shown here:

$$C_D = \frac{F_D}{\frac{1}{2}\rho V_\infty^2 A_{ref}} \quad (3.8)$$

$$C_L = \frac{F_L}{\frac{1}{2}\rho V_\infty^2 A_{ref}} \quad (3.9)$$

Here F_D is aerodynamic force in stream wise direction and the force component which is normal to this direction is F_L appropriate directions and velocity (V_∞) which is upstream velocity, flow density (ρ) and reference area (A_{ref}) are set by environment and the case study cross section. In turbulent model due to the periodic vortex shedding the pressure is also oscillating in time show and it has effects on

drag and lift coefficient. In this picture we can see an example of force coefficient oscillation in 1s.

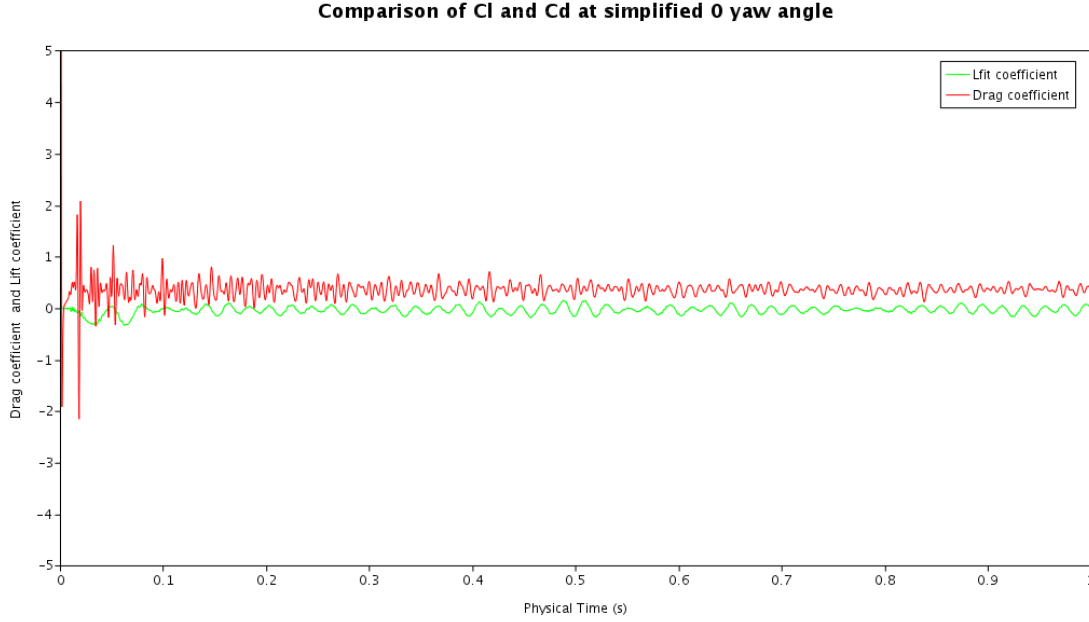


Figure 3.1: The history of the drag and lift coefficients obtained for the simplified sail mast in 1 second physical time to be compared

The lift and drag are related to growth of vortex at the back of the sail mast which is downstream. Lift coefficient is oscillated by vortex shedding frequency and as the graph shows drag is oscillated around two times of this frequency.

λ_2 criterion and Q criterion

Velocity gradient tensor is defined by $D_{ij} = \frac{\partial u_i}{\partial x_j}$. The velocity gradient tensor can be decomposed into two parts symmetric and skew symmetric part.[11] Where S_{ij} is strain rate tensor and Ω_{ij} is vorticity tensor.

$$D_{ij} = S_{ij} + \Omega_{ij} \quad (3.10)$$

$$S_{ij} = \frac{1}{2} \left(\frac{\partial u_i}{\partial x_j} + \frac{\partial u_j}{\partial x_i} \right) \quad (3.11)$$

$$\Omega_{ij} = \frac{1}{2} \left(\frac{\partial u_i}{\partial x_j} - \frac{\partial u_j}{\partial x_i} \right) \quad (3.12)$$

The characteristic equation for ∇u is shown as:

$$\lambda^3 + P\lambda^2 + Q\lambda + R = 0 \quad (3.13)$$

which Q represents the local balance between vorticity magnitude and shear strain rate and λ_2 looks for pressure minimum but without unsteady straining and viscosity. So by considering $S^2 + \Omega^2$, a vortex is defined as a connected region with two negative eigenvalues of $S^2 + \Omega^2$ and λ_2 it leads to find out there is strong correlation to the noise generation.[14]

3.2 Turbulent flow

Turbulence flow is a type of fluid (gas or liquid) in which the fluid undergoes irregular fluctuations, or mixing, in contrast to laminar flow, in which the fluid moves in smooth paths or layers. The problem with turbulence is that although it has been widely studied no one can actually explain or fully predict the exact behavior of the flow. In addition in turbulent flow the speed of the fluid at a point is continuously undergoing changes in both magnitude and direction that should be considered to analyze it.[19]Turbulence flow can be visualized as consisting of irregular swirls of motions called eddies which consist of many different size and affects on each other.[19] A few characteristics are typical and could define a turbulent flow:

- Irregularity: the flow seems irregular and chaotic but is assumed to be governed by the Navier-Stokes equations creation of turbulent eddies and the destruction in the cascade process together with dissipation.
- Diffusive and dissipation: increased tendency to spread and blend with nearby flow and mixing of boundary layer delaying the separation. The largest eddies draw kinetic from the flow and the energy is transferred from larger to smaller eddies and finally turned into thermal energy at the smallest eddies. The process is also known as the cascade process.
- Three-Dimensional: turbulent flow is by nature always three-dimensional although it could be modeled as two-dimensional if the equations are time-averaged. And in the thesis simulations are going to run by RANS,URANS, and DES that show we need to have three dimensional model to analyze our data to get aero-acoustic parameters.

We can see in the picture that the turbulent flow is shown at the downstream of the simplified sail mast which is colored by pressure. The turbulent kinetic energy is strongly related to turbulent flow strength which is combination of fluctuations of velocity in different directions. If we look at the real life it is difficult to find a laminar flow in real life and so turbulent flow is really connected to our life and so a lot of research have been done to find out how is the behaviour of this kind of flow and aero-acoustic can be one of this part of research interests that a face to turbulent flow behavior.

$$K = \frac{1}{2}(\overline{u'^2} + \overline{v'^2} + \overline{w'^2}) \quad (3.14)$$

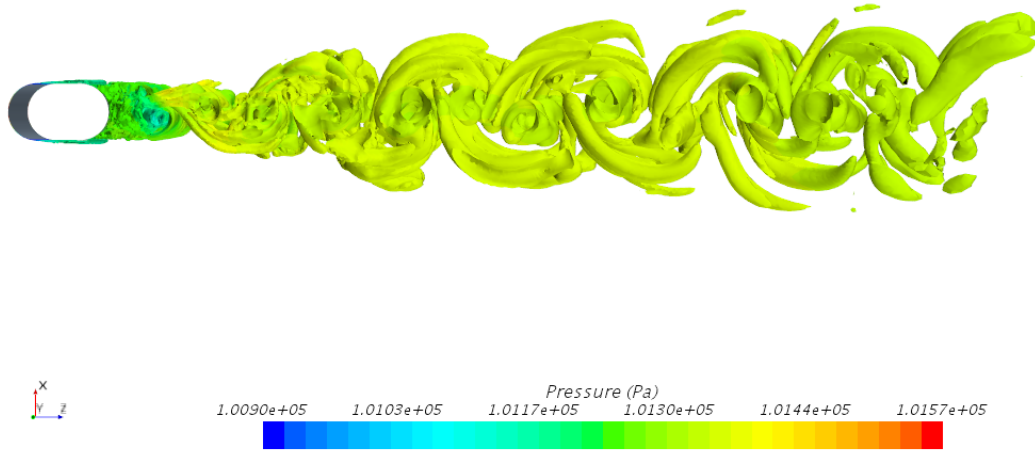


Figure 3.2: Turbulent flow on downstream of simplified sail mast at $\psi = 0^\circ$ colored by pressure in range of 1.009×10^5 (Pa) and 1.0157×10^5 (Pa)

3.3 Acoustic theory

Acoustic was originally the study of small pressure waves in air which can be detected by human ear: sound[18]. Sounds are a product of all human activities and are all around us. Sounds can be pleasant and useful but they can also be a serious threat to our health and specially our ear. Understanding how to deal with sound is crucial for the future sustainability of our living environment and these years acoustics field has made companies and whole industries more aware of the effects of noise on their customers, so today acoustics is an important aspect in product development.

Equation of Acoustics can be explained by Decibel scale which is used to measure the intensity of a sound pressure p .

$$20 \times \log_{10}\left(\frac{|p|}{p_{ref}}\right) \quad (3.15)$$

The reference pressure $p_{ref} = 2 \times 10^{-5} \frac{N}{m^2}$ and we consider $p = p_0 = 1atmosphere(= 10^5 \frac{N}{m^2})$. By looking at back and forth motion of the fluid at the acoustic particle velocity ν we can find that there is a relation between acoustic pressure, density, and speed of sound.

$$acoustic\ particle\ velocity = \frac{acoustic\ pressure}{density \times speed\ of\ sound} \quad (3.16)$$

In most of study cases the amplitude of acoustic is small compare to the mean pressure p_0 , and by linearizing the equations we start to analyze sound propagation. So we start to consider sound propagating in a stationary inviscid fluid of mean pressure p_0 and density ρ_0 and comparison between oscillation p', ρ' and mean value

of them show that they are very small. Here fundamental equations of fluid dynamic and effect of sound propagating are shown. Momentum equation can be written in this form:

$$\rho_0 \frac{\partial v}{\partial t} + \nabla p' = F \quad (3.17)$$

Continuity equation can be written in by volume source distribution $q(x, t)$ that is the rate of fluid volume per unit volume of the fluid.

$$\frac{1}{\rho} \frac{D\rho}{Dt} + div v = q \quad (3.18)$$

$$\frac{1}{\rho_0} \frac{\partial \rho'}{\partial t} + div v = q \quad (3.19)$$

Now by removing v we have:

$$\frac{\partial^2 \rho'}{\partial t^2} - \nabla^2 p' = \rho \frac{\partial q}{\partial t} - div F \quad (3.20)$$

By this equation we can find the pressure p' and undistributed and distributed states are:

$$p_0 = p(\rho, s), s = constant \quad (3.21)$$

$$p_0 + p' = p(\rho_0 + \rho', s) = p(\rho + s) + \left(\frac{\partial p}{\partial \rho}(\rho, s) \right)_0 \rho' \quad (3.22)$$

The derivative is evaluated at the undistributed values of the pressure and density (p_0, ρ) . The dimension of speed of sound is square of $\left(\frac{\partial p}{\partial \rho} \right)_s$ Where the derivative is taken with the constant entropy s which we have from undisturbed fluid. The heat transfer between fluid particles by viscous and thermal diffusion are neglected during the passage of a sound wave.

$$\left(\frac{1}{c_0^2} \frac{\partial^2}{\partial t^2} - \nabla^2 \right) p = \rho_0 \frac{\partial q}{\partial t} - div F \quad (3.23)$$

Whenever we find prime(t) on the acoustic pressure it means that this equation control the production of sound waves by reference volume q and the force F . When we do not have these parameters the equation shows sound propagation from sources of sound which are on the boundaries of the fluid. The reference volume q and the body force F would not be appear in a complete sound generation in a fluid. These parameters get to involved when we want to model the real sources of sound in terms of volume sources and forces. This is very important that we specify the sources of sound correctly because if it is specified by some small error it leads to large errors in sound predictions. This is because only small fraction of the energy of a vibrating fluid radiates away as sound. When $F = 0$ and $v = \nabla \phi$ in the momentum equation the pressure perturbation is given by :

$$p = -\rho_0 \frac{\partial \phi}{\partial t} \quad (3.24)$$

So the following equation appear that velocity potential is the solution of which leads to this wave equation of classical acoustics. Speed of sound in air is shown in the table

$$\left(\frac{1}{c_0^2} \frac{\partial^2}{\partial t^2} - \nabla^2 \right) \phi = -q(x, t) \quad (3.25)$$

C_0	$\frac{m}{s}$	$\frac{ft}{s}$	$\frac{km}{h}$	$\frac{mi}{h}$
Air	340	1100	1225	750

Table 3.2: Speed of sound

From the acoustic point of view sound and noise constitute the same phenomenon of atmospheric pressure fluctuations about the mean atmospheric pressure but what is sound to one person can be noise to somebody else.[12] If we focus on noise which is a modern research topic in different type of industries. Type of noise can be divided to steady, non-steady or impulsive which depends on variation of sound pressure level. Steady noise is a noise with negligibly small fluctuations of sound pressure level within the period of observation.[12] A noise is called non-steady when its sound pressure levels shift significantly during the period of observation. Furthermore Intermittent noise and fluctuating noise are two type of this kind of noise. Fluctuating is a type of noise which the level changes continuously and to a large extent during the period of observation.[12] When the noise level drops to the level of the background noise for some times during the period which we considered this kind of noise is called intermittent. The time period which the level stay at a constant level different from ambient background noise have to be one or a few seconds. In addition this kind of noise is characterized by the ambient noise level, level of the intermittent noise, and the average duration of the on and off period. All these levels are changing with time and the intermittent rate is varying as well and this type of noise is usually assimilated to a fluctuating noise as impulsive noise. Impulsive noise includes one or a few bursts of sound energy, each of a period is less than one second.

It is very important for us to find if our cases generate tonal noise or not because in previous researches students could not find any tonal noise from sail mast. This type of noise can be continuous or fluctuating and is characterised by a few single frequencies that is very different from broadband noise which is characterised by energy at different frequencies and of the same sound pressure level as the tonal noise. In order to find tonal noise we need to search for single impulse in the sound pressure level graphs.

Aero-acoustics research topic deals with the sound generated aerodynamically and make strong connection between acoustic and fluid dynamic research areas. It is derived from the classical wave equation with a source term and aerodynamic parameters are going to be added. Several analogies for analyzing aero-acoustic features exist and most of them are based on the Lighthill acoustic analogy. Aero-acoustic noise generation in a simple manner can be explained by the flow interacting with geometrical irregularity like a boat or sail mast. There is a variety of applied problems where aero-acoustic phenomena are the major contributors to noise, i.e. aircraft engine noise, propeller noise, rotor noise, noise of fans in whatever application, cavity noise, tones of wires and cylindrically shaped bodies in transverse wind, airframe noise at aircraft, high speed trains and cars, noise in valves and nozzles, etc.[7]

As an example interaction of flow in wake region creates unsteady turbulent flows which are often detached and thus in turn generates noise. A major problem of fluid dynamics is that the equations of motion are non-linear and this implies that an exact general solution of these equations is not available. Acoustics is a

first order approximation in which non-linear effects are neglected and turbulence is a chaotic motion dominated by non-linear convective forces which means accurate deterministic description of turbulent flows is not available.

FW-H theory of sound generation by turbulence is used here and the key of this theory is use of integral equation, which is much more suitable to introducing approximations than a differential equation. Hence, in order to fully estimate the aeroacoustic noise one has to use CFD-tools is called Computational Aero-Acoustics(CAA) and the computational theory of the thesis is based on CAA, that is mixture of acoustic theory and CFD.

3.4 Computational Method theory

The governing equations of the continuity, energy and Navier Stokes are well known in fluid dynamics and they were mentioned before. In general form continuity, Navier-Stokes and Energy equation are shown respectively.

$$\frac{d\rho}{dt} + \rho \frac{\partial v_i}{\partial x_i} = 0 \quad (3.26)$$

$$\rho \frac{dv_i}{dt} = -\frac{\partial p}{\partial x_i} + \frac{\partial}{\partial x_j} \left[\mu \left(\frac{\partial v_i}{\partial x_j} + \frac{\partial v_j}{\partial x_i} - \frac{2}{3} \frac{\partial v_k}{\partial x_k} \delta_{ij} \right) \right] + \rho f_i \quad (3.27)$$

$$\rho \frac{du}{dt} = \sigma_{ij} \frac{\partial v_i}{\partial x_j} - \frac{\partial q_i}{\partial x_i} \quad (3.28)$$

ρ is density, v velocity, t time, x length, μ absolute viscosity, p pressure, u internal energy, q conductive heat flux, σ stress tensor and f body force.

In computational fluid dynamics (CFD) the variables of a flow field are solved for inside a domain of interest using a computational software. The domain discretized into a number of finite volumes or cells in which the governing equations are solved in an iterative process. The finite volume method is used to discretize the transport equations of continuity, momentum and energy the segregated flow solver is used to solve these equations. The flow equations one for each component of velocity and one for pressure is a segregated or uncoupled way and the link between momentum and continuity equations is achieved with a predictor corrector approach.

3.4.1 Computational Fluid Dynamics (CFD) and Computational Aeroacoustics (CAA)

Flow can be described by partial differential equations which we can not solve it analytically to obtain the solution numerically we have to use a discretization method which approximate the differential equations by mathematical equations which can be solved by computer. The model is divided in small part which the approximations are applied in these small parts in space and time and then the numerical solution provides results at discrete locations in space and time. The quality of discretizations is very important because it leads to accuracy of numerical solutions. The complicated geometries force engineers to use CFD when they can not solve by standard methods. In the project the CFD method is used to solve the

equation of fluid motion in three dimensions and use this tool to simulate turbulence flow which generates noise.[8]

Here can be mentioned that an experiment is much more expensive compared with a CFD simulation. On the other hand we can have complete knowledge of the flow in all position of the computational domain. Computational Aero-Acoustic(CAA) is a mixture of acoustic theory and CFD, it is concerned with prediction of the aerodynamic sound and the transmission of the generated sound starting from the time dependent governing equations. The full, time dependent, compressible Navier-Stokes equations describe these phenomena.[15] By considering computational costs in the engineering applications Computational aero-acoustics(CAA) is faced to predict the accurate far-field noise, where the sound wave in long distance transmission is often characterized as fluctuations with small magnitudes.[24] The hybrid methodology is a very common acoustic computational method to predict the far field noise that is generated by aerodynamic flow. From looking at different kinds of simulations can figure out that the cost of Direct Numerical Simulation (DNS) and Large Eddy Simulation (LES) is too high and also Reynolds Average Navier-Stokes (RANS) equations do not provide instantaneous flow fluctuation so our final choice is Detached Eddy Simulation (DES) but the simulation was started by RANS model to get all the aerodynamic features around the case studies to see how boundary layer is going to be made and then it was changed to DES model which could give us turbulent flow features for make a link to acoustic part.

3.4.2 Ffowcs Williams Hawkings (FWH) acoustic analogy

Before starting the main part of simulation some theories are covered in this section. For analyzing noise generation in turbulent flows we need to utilize computational aeroacoustics field and this part is mainly divided in two sections Direct Numerical Simulation(DNS) approach to Computational Aero-Acoustics(CAA) and Hybrid approach but as it was mentioned before that Direct Numerical Simulation (DNS) is expensive so the hybrid approach is applied for this project. The dominant parts of this approach is integral methods that covers Lighthill's analogy, Kirchhoff integral and Ffowcs Williams Hawkings(FW-H). The Ffowcs Williams and Hawkings (FW-H) formulation, the contribution of solid wall to noise is derived in the form of integral over the wall of sail mast.[24] The general solution for wave propagation is getting integral over all noise sources. So to use FW-H formulation a form of integral over a permeable surface is used and it is located around the sources of noise and this surface calculate the sound pressure in receivers locations by using Farassat's Formulation 1A.

We can see all kind of sources of noise are used in FW-H formulations but the volumetric sources outside of permeable FW-H surface is not counted in the formula. The noise sources are implied in the equations as the perturbations of the pressure, momentum and mass through the surface. If we have moving control surface $S(t)$ we can use Ffowcs Williams and Hawkings. The main part is to include the effect of the surface in differential equation. Here $B(t)$ enclosed by the surface $S(t)$ and this is shown in different cases.[20]

$$\left\{ \begin{array}{ll} h(x, t) < 0 & \text{if } x \in B(t) \\ h(x, t) = 0 & \text{if } x \in S(t) \\ h(x, t) > 0 & \text{if outside } B(t) \end{array} \right\}$$

By choosing a physical quantity defined outside $B(t)$ and extend the definition for all space to multiply it by the Heaviside function $H(h)$ a new variable is created and is equal to the physical quantity outside of the $B(t)$. So now we can extend the equations to the whole space by adding surface sources, The surface $S(t)$ is defined by time and space and by applying the Green's theorem and using free space Green's function we have This equation here:

$$\begin{aligned}
p'(x, t) = & \frac{\partial^2}{\partial x_i \partial x_j} \int_{R^3} \left[\frac{(\rho v_i v_j - \sigma_{ij}) H}{4\pi r} \right]_{\tau=t_e} dV_y \\
& - \frac{\partial}{\partial x_i} \int_{R^3} \left[\frac{f H}{4\pi r} \right]_{\tau=t_e} dV_y \\
& + \frac{\partial^2}{\partial t^2} \int_{R^3} \left[\frac{(p'/c_0^2 - \rho') H}{4\pi r} \right]_{\tau=t_e} dV_y \\
& + \frac{\partial}{\partial t} \int_{S(t_e)} \left[\frac{\rho_0 b \cdot n}{4\pi r (1 - M_r)} \right]_{\tau=t_e} dS \\
& - \frac{\partial}{\partial x_i} \int_{S(t_e)} \left[\frac{p' n_i - \sigma_{ij} n_j}{4\pi r (1 - M_r)} \right]_{\tau=t_e} dS
\end{aligned} \tag{3.29}$$

H is Heaviside function, n is normal vector, $r = ||x - y||$ is the distance from a source point on the surface to the observer, $M_r = \frac{b \cdot (x-y)}{rc_0}$ is the Mach number of the surface and the subscript r indicates the projection of a vector quantity in the radiation direction. The subscript t_e indicates that the integrals are evaluated at each sources related time(emission time), given by $\tau = t - \frac{|x-y|}{c_0}$, where y is the source location, t and x are the observer time and position, respectively.[3] The flow around the surface are related to the first three integrals and the last two items show thickness noise and sound generated by surface forces.

$$\begin{aligned}
p'(x, t) = & \frac{1}{4\pi} \frac{\partial}{\partial t} \int_{S(t_e)} \left[\frac{\rho b \cdot n}{r(1 - M_r)} \right]_{\tau=t_e} dS \\
& - \frac{1}{4\pi} \frac{\partial}{\partial x_i} \int_{S(t_e)} \left[\frac{p' n_i}{r(1 - M_r)} \right]_{\tau=t_e} dS
\end{aligned} \tag{3.30}$$

The source parts in the equation is evaluated using time accurate aerodynamic flow field result which found from the CFD calculations. And sound sources can be shown in terms of the time dependent flow field that is calculated before.

3.4.3 Prediction of noise

For solving our turbulent flows some principle numerical model can be used Direct Numerical Simulation (DNS), Large Eddy Simulation(LES), Detached Eddy Simulation (DES) and Reynolds Average Navier stocks Simulation (RANS). These are the main models that turbulent model can be solved. In turbulence flow studies the ultimate object is to reach a tractable theory or model that can be used to

calculate quantities of interest. The first numerical model DNS is only used for low Reynolds Number to solve all scales of turbulent flow. We can say the most expensive way that can be used for solving the Navier Stokes equation is DNS that solves whole turbulence scales without predictions.

LES is large three-dimensional turbulent scale, is volume averaged and it avoids smallest scales to reduce computational cost by averaging cross time and space and this removes information of small scale that are expensive to solve in numerical computation, and large eddies are represented explicitly, so it can be expected to be more accurate and reliable than RANS if large scale unsteadiness is investigated [4]. But It is still very expensive.

DES approach is a combination of classical RANS and LES method and it is based on the idea of converging the boundary layer and solving scales near the wall by a RANS model and Switching to the LES mode in detached regions of the turbulent flow which is far from the walls. So this approach came out because of difficulties related to LES models specially near wall region that result in development of hybrid method to combine RANS and LES models. The DES approach may be used with any turbulence model that has an appropriately defined length scale of turbulent flow and is sufficiently localized model. To predict the noise we need to use DES because by RANS we can not have enough details about separated flow and in RANS formulation there is no information about turbulent flow structures. If we look at the Reynolds Decomposition. We can see U is the averaged value of the flow velocity and u' is the fluctuation of the flow. RANS models all turbulence scales, It is time-averaged. Thus making it faster than other methods to compute but RANS only solves the largest scale that represent the mean value of the velocity. So this method can be interesting for the first determination of general parameters not finding some details like turbulent flow features.

$$u = U + u' \quad (3.31)$$

The main turbulence models which are common in simulating turbulent flow are the $k - \epsilon$ and $k - \omega$. The $k - \epsilon$ model is more suitable when you are studying free shear layers and wake region and the standard $k - \omega$ model provides more accurate solutions in the near wall boundary regions. There is also an improved version of the $k - \omega$ which we have used in this project called $k - \omega - SST$ in which $k - \epsilon$ and $k - \omega$ models activated automatically over the domain and we can study the flow behavior near and far from the wall to have some results near sail mast and also far from the sail mast for having aero-acoustic data.

Chapter 4

Computational setting

The main part of the computational setting is divided to three sections pre-processing, simulation and post-processing. The commercial software STAR-CCM+ is used for all these parts and two cases of different yaw angles 0 degree and 90 degree are investigated here, first case the mast with a cavity inside and without cavity to show the main source of noise.

4.1 Pre-processing

The quality of the final result is highly dependent of the work done prior to run the simulation. So the setting and mesh design are extremely important which a lot of time consumed for theses parts. The 3D models of sail masts and the computational domain are drawn and assembled by commercial software STAR-CCM+.

4.1.1 CFD domain and physics setup

The design features are visualized here to show how they installed for simulations. The outer domain is formed by a coarser mesh while the inner domain has a finer mesh. These features were applied in order to capture the small-scale turbulence flow structures back of the sail mast and on downstream flow region. We locate a surface around the inner part which is called FW-H surface and it should cover around the noise sources. And at the begining of the simulation we need to consider RANS model should be set to define the turbulent flow field structure around the wall at this idea comes from theory and research experiences which says RANS is a suitable model to determine the flow features near the wall.

In general it is necessary to use a enough large domain for numerical calculating of acoustics because some regions like near wall, wake region, and far field should be consider to get complete flow features from our simulations. In addition the pressure fluctuations that are made by the sail mast are sensitive to distance from the main sources of noise generation so it is very important to consider enough space for downstream of the sail mast which leads to better investigation. However, it should be mentioned that reflected noise also has affect on the results.

By considering air as a ideal gas and the compressible flow here, the finite volume method is utilized to dicretize the continuity, momentum and energy equations.[1] The numerical methodology of the compressible $k - \omega$ SST DES introduced and the

methodology is set up as follows. Furthermore the segregated flow solver is used to solved discretized equations and Hybrid-BCD is used for computing convection flux on a cell face and the gradient computation is set to Hybrid Gauss-LSQ .

The modes that are set for the simulation are shown here: Three dimensional model is set for the project to analyze the flow close to real case. The type of flow is ideal gas and Segregated flow is used here which solves the flow equations one for each component for velocity and one for pressure and segregated fluid temperature was also considered. Implicit unsteady, Detached eddy simulation, SST(menter) $K - \omega$ detached eddy are applied to solve the turbulent flow. Ffowcs Williams-Hawkings unsteady, On the Fly FW-H is set to solve the acoustic part of the project and It is difficult to ensure that the values of Δy^+ of all elements nearest the walls are above a high value or below a small value. So This problem is solved with the approach of all y^+ wall treatment, which modifies the specific dissipation rate in the near wall elements.[21]

The computation domain constructed for the simulation is shown here. The length of computational domain is $8m$ and the mast is located $3m$ from the inlet and $5m$ from the outlet. The size of computational domain is designed by considering of getting propagation waves in the far field and the flow direction is aligned with z-axis.

Parameter	R	r	L	W	D	d	T
Dimension(m)	3.1	0.63	5.2	2.7	0.27	0.15	0.5

Table 4.1: Case dimensions

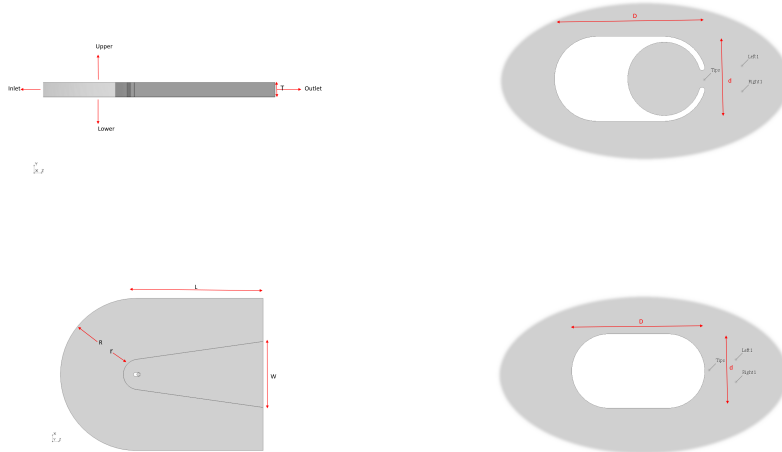


Figure 4.1: computational domain and sail mast dimensions which are shown by top and side view

Moreover under-relaxation factors in DES numerical model are set for velocity and pressure parameters during the iterations to guarantee the stability of equations in iteration process these numbers were set 0.2 and 0.8 for pressure and velocity respectively but for RANS model they were 0.3 and 0.7, these values need to be between 0 to 1. To achieve stability in numerical process the time step is set to 10^{-4}

and maximum number of iteration is at every time step is set to 10 for converging the solution.

Beside previous setups symmetry conditions are applied for the acoustic domain and Condition of velocity applied for the inlet and pressure for the outlet. In addition we have to keep in mind that sail mast is the only part that is set as wall surface inside of computational domain. And time marching procedure was done by using the implicit second order accurate and here $n+1$ and n indicate the new and old time iteration respectively.

$$\left(\frac{\partial\phi}{\partial t}\right)_{n+1} = \frac{3\phi^{n+1} - 4\phi^n + \phi^{n-1}}{2\Delta t} \quad (4.1)$$

$$\phi_{new} = (1 - \alpha)\phi_{new} + \alpha\phi_{old} \quad (4.2)$$

Where ϕ_{new} is the value of the equation at current iteration, ϕ_{old} is the value of the equation at the previous iteration and α is the value of the parameters.

4.1.2 Mesh generation method

The mesh generation is done by directed mesh function from top layer to bottom layer of the connected computational domain, the polygonal and prism layer mesh are the properties of the mesh. The prism layer mesh is used to accurately resolve the near wall flow and it consists if 12 layers and with the $0.0015m$ total thickness near the wall and from past research experiences and simulations polygonal mesh is the best type of mesh to get noise generated by the case studies along the computational domain. In the Figure 4.2 the prism layers are shown near the sail mast tips to giving well enough Y^+ which approximately 1. Y^+ is normal wall resolution which is defined by wall shear stress(τ_{wall}), the distance between center of closest cell to the wall(y) and kinematic viscosity(ν):

$$Y^+ = \frac{yu_\tau}{\nu}, u_\tau = \sqrt{\frac{\tau_{wall}}{\rho}} \quad (4.3)$$

The instantaneous contours of Y^+ of the near wall cells were checked and can be seen that the small Y^+ shows the well solved boundary layer and means it is in turbulent sublayer region.

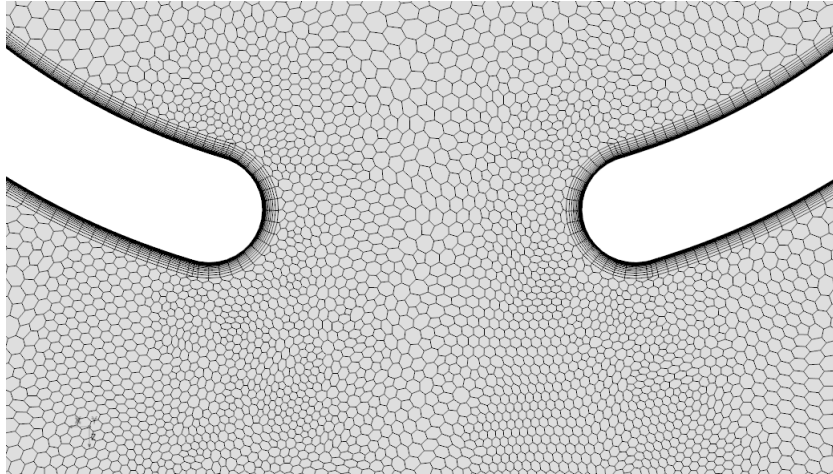


Figure 4.2: Prism layers located around sail mast's tips

	Semi elliptic($\psi = 0$)	Semi elliptic($\psi = 90$)	Sail mast($\psi = 0$)	Sail mast($\psi = 90$)
Number of cells[millions]	3.5	3.5	7.5	7.5
Number of Vertices[millions]	7	7	15	15
Time steps	10^{-4}	10^{-4}	10^{-4}	10^{-4}
Velocity of inlet [$\frac{m}{s}$]	20	20	20	20

Table 4.2: Mesh characteristics

In 3D simulations, as in this case, three main mesh types are hexahedral, polyhedral and tetrahedral. Tetrahedral is the simplest one and others are built from several tetrahedral cells. In the simple mesh generation the results are fast but there is lack of accuracy when solving actual problem. The main advantage of polyhedral meshes is that they have many neighbors, so gradients can be better approximated. But it needs more storage and computations. In addition the convergence properties are better in computations on this kind of mesh.

To find suitable mesh for performing the simulations, some parameters needed to be taken into account. The mesh should have between 15 to 25 million vertices. This was to ensure that the computational resources provided were used effectively. Also the mesh needed to be fine enough in the area where small-scale vortex shedding occurs which is wake region, so at the final point the mesh at the wake region is refined by increasing the cells and the surface growth rate ratio is set to 1.05, The length, angle and cell growth rate of the refinement region are controlled. This area is considered because it can be the most important part of noise generation from the mast's tip and downstream of the sail mast.

In order to have good aero-acoustic results around 7.5 millions cells are generated for the sail mast with the tips and 3.5 millions cell for the simplified sail mast. To resolve the acoustics, the cell size must be small enough and the good estimation can be at least 20 cells per wave-length is preferable. The cell size can be $\Delta C = \frac{C_0}{20f_{whistling}}$ This cell size was desirable to transport the sound correctly in the inner domain because the error decreases as the number of cell faces increases. In Aero-Acoustic simulations, a large number of iteration is in general required in order to have a appropriate solution. So according to this point of view polyhedral mesh was the most suitable candidate due to a higher accuracy at a shorter computational time. But the high accuracy need to spend more time for mesh generation and mesh dependency studies. In order to generating mesh the directed mesh selected as mesh generation because in this method is easy to control the number of cells and the mesh is faster to compute in comparison to other used methods.

To get the data from mesh domain some drive parts are put in the model. The probes were inserted into the domain to measure velocity and pressure to later be able to compute the results. The plan was to choose the one mesh and apply for different configurations in 0° and 90° and refine the wake region of the case studies. Unfortunately problems were encountered regarding finding a convergence solution. And a lot of time was spent on fixing this and when at final point 3.5 and 7.3 million cell mesh were used for sail mast without cavity and sail mast with cavity because of sail mast's tips.

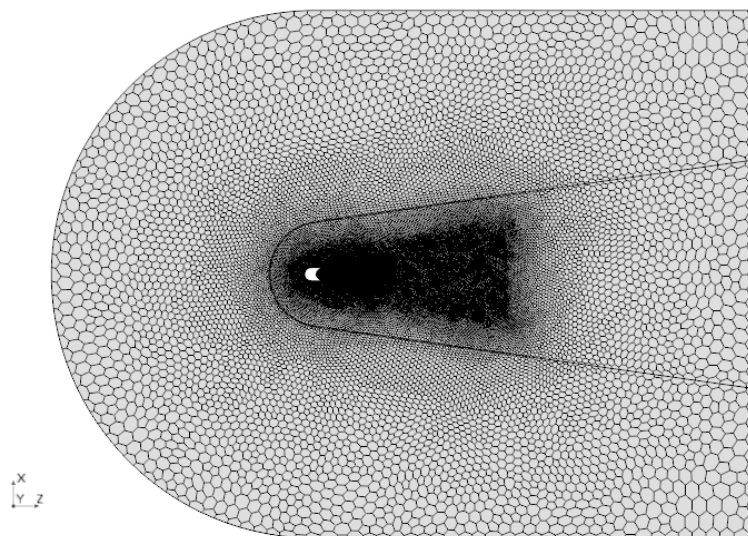
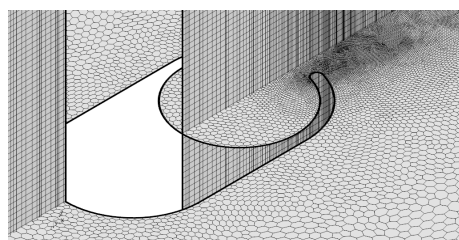
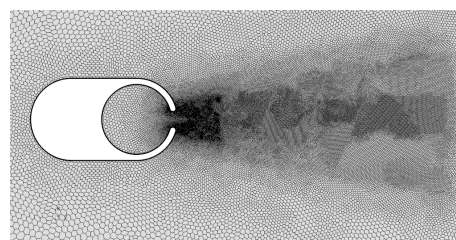


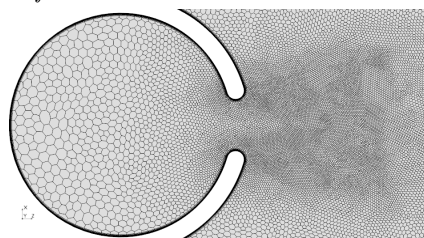
Figure 4.3: Mesh design of whole computational domain with the sail mast at $\psi = 0^\circ$



(a) Spanwise direction mesh generation for sail mast at $\psi = 0^\circ$ which is refined



(b) Mesh generation of wake region which is refined



(c) Refined mesh around sail mast's tips

Figure 4.4: Refinement part of mesh design

4.1.3 FWH permeable surface and far-field microphones

A permeable Ffowcs Williams Hawkings(FW-H) surface is located on a fine region of the mesh around the sail mast and in computational domain to cover all the noise sources and the CFD computations are extracted from FW-H surface . The exact location of FW-H surface is where the inner part and outer part are connected. Furthermore when we put the permeable FW-H surface on-the-Fly models calculate the sound pressure at far field by 36 receivers with Farassat's Formulation 1A formula which is solution of Ffowcs Williams Hawkings(FW-H) in subsonic region.

Around the domain, 36 FW-H receivers are placed in circle with a 10m radius in the plane of $y=0$ to get the far field noise. The center of the circle is placed at the origin of the coordinate system and the specific microphones of $0^\circ, 90^\circ, 180^\circ$ and 270° are located at the position with coordinates of $(x,y,z)=(0,0,10), (10,0,0), (0,0,-10)$ and $(-10,0,0)$ respectively to be shown in the results section. The acoustic transport equations are decoupled from the flow equations so it is possible to place the receivers out of the computational domain.

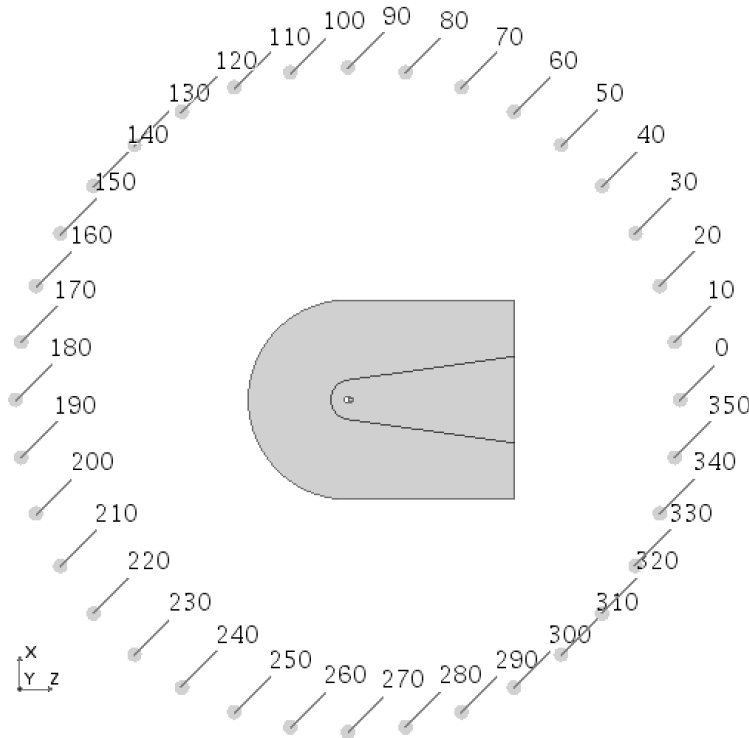


Figure 4.5: Location of Receivers around the computational domain by radius of 10m

4.2 Post-processing

According to show the final results post processing should be done because the important part of the project is the result and the plots need to be compared with each other. When simulations had reached sufficient convergence the results were extracted with a variety of tools.

- Plane section: a plane section is a slice cut through the computational domain where results can be presented and it is very good when a visualization of

gradients or a full spectra. So in this project two surfaces are put to show some values along computational domain and these two surfaces are along spanwise and streamwise direction to show better view of 3D computational process.

- Isosurfaces: when a specific value is evaluated within the domain an isosurfaces is useful to visualize areas where that value can be found and here wake region is the interesting part to show isosurfaces.
- Streamline: this is especially useful when one want to see how specific particles move through the flow. So velocity and pressure can be useful to plot by this type of tool.
- Probe and receivers: velocity and pressure are extracted from the probes which are located near wall of sail mast and receivers get the far-field noise around the computational domain to plot it.

4.2.1 Fast Fourier transform and sound pressure level

Data set functions apply signal processing to sets of wave data. There are two kinds of data that are used for signal processing:

- Histories, which collect data at specified locations that are organized into points,lines,or surfaces.
- Transforms, which are either Fourier transforms or inverse Fourier transforms. Fourier transforms derive frequency data from signal data and Inverse Fourier transforms derive signal data from frequency data.

For signal processing in particular, any signal can be represented either in the time or the frequency domain. These representations are equivalent, that is, $S[T] \equiv S[F]$. Fourier transforms are used to transform a signal from the domain to the frequency domain, and inverse Fourier transforms are used to do the reverse. Transforming a signal to the frequency domain makes it possible to identify the dominant modes in the signal.

At the validation point the plot of pressure against time at a location set some distance from the mast are plotted for 4 cases that 36 receivers are located around the mast. These measurements are used in frequency analysis to identify the dominant modes for the signal and the frequency bands containing these modes. Large modes within the range of frequency audible to human hearing would suggest a noisy environment. Comparing the predicted modes to the measured modes gives an understanding modes gives an understanding of the uncertainty that is associated with the simulation. If uncertainty is within acceptable levels, further simulations could be performed for varying configurations of the sail mast and these simulations would investigate ways of reducing the dominant modes, or at least moving out of the range of human hearing.

The receivers record the pressure fluctuations over time and the FFT algorithm transforms the time dependent signals from the time domain into the frequency domain. After the FFT the Sound Pressure Level(SPL) was plotted as function of frequency to distinguish tonal peaks in the signal. Low frequency noise is filtered out in the similar way as in the human ear.

We put the probes to show that noise is generated from vortex shedding produced by the cavity of the mast and we can monitor the static pressure. FFT algorithm computation was then performed on the pressure time history from the probes. This procedure was similar to that of the data obtained from the receiver. The difference is that instead of the SPL, the Power Spectral Density(PSD)was computed. PSD describes the signal power per unit frequency and is used to characterize random processes in the frequency domain and applies to stationary random processes and it is sometimes also referred to as a power spectrum. If a pressure peak is present in the SPL from the receivers, a similar peak should appear in PSD from the probe data. This would imply that the noise is generated in the region of the probe.

4.2.2 Plotting results

The residual plot is created automatically once the simulation starts iterating. In order to investigate the results Monitor plots that can display data from monitors,data set functions and/or tables are plotted. There is two kind of plots which have been used here are:

- Monitor plots that are user created plots and the residual plot that is generated and modified automatically by the system.
- XY plots that display solution data from the simulation and table.

The plots were created before,during and after i run the simulation. Plus the quantities are plotted in different type of plots. After preparing the relevant report a plot and monitor are created. In a default monitor plot,the y axis uses any one of various monitors while the x axis represents solution progress. (The x-axis uses the iteration monitor in a steady simulation and the physical time monitor in an unsteady one). So most of the plots here are shown by physical time because our simulations are unsteady.

XY plots can display data from model parts such as boundaries or derived parts such as line and point probes. For most scalar fields vertex values are interpolated from cell values, and thus data extraction with the smooth filled option is more expensive in terms of computing power. In addition for the velocity profile along the model a line probe is created from inlet to outlet of the mast and then refer to the part in a XY plot. Moreover The line probe is located at the mid of sail mast in Z direction by 100 resolution. The X type is defined by vector quantity that is Z direction and Y type is shown by smooth values and the line probe linearly interpolates from values that are located at the vertices of the region. These values are computed by averaging cell centre values from neighboring cells.

Chapter 5

Results

In this section results of four simulations carried out are presented. The simulations are done on cluster provided by Swedish National Infrastructure for Computing (SNIC) for numerical investigation.

In particular descriptions and visualizations of the flow features, signal analysis of velocity and pressure signal sampled by monitoring point are reported for different yaw angles, $\psi = 0^\circ$ and $\psi = 90^\circ$. For each yaw angle there is two simulation and in total they are four different simulations. After the first simulations which were done for the sail mast at $\psi = 0$ other cases were prepared to be investigated. This chapter is divided in two parts flow characteristics and acoustic sound source. But the most focus is on aero-acoustic part which is the aim of the thesis to be analyzed.

5.1 Flow characteristics

To understand the mechanics of aero-acoustics, some characteristics of the flow are necessary to investigate here the characteristics of pressure, velocity and vorticity are going to be shown because of the connection between vortices that are generated by the bluff bodies and cavity this part starts to show how main parameters are changed along the case studies and which part of sail mast has impressive impact on vortex generation. Starting from boundary layer and separation of it lead to have different wake region on downstream of the computational domain. Because of significant cross section of these case studies we can look at it like a bluff body which vortices are shed periodically behind the bodies.

5.1.1 Velocity

To simply the understanding of noise generation the velocity contour plot is analyzed and presented here the results are shown in four cases and two different yaw angles. In the simplified sail mast 3.5 millions and in the sail mast 7.5 million cells are generated. A wake pattern is formed downstream of the sail mast and shows a Von Karman vortex street, the vortex street is caused by the unsteady flow separation. From Figure 5.3 most of the vortices in the wake are created from the bluff body and not from the tip geometry except in Figure 5.4 it can be shown that tip location has some affect on generation of the vortices. There is also some differences between case *a* and *b* in both yaw angles, vortices are created earlier in case *b* rather than case *a* so this phenomena can be explained by existence of the

tips because by plotting streamline in streamwise direction it could be find the flow goes into the cavity and it has low velocity magnitude value. Further more there is more unsteadiness in the case which the sail mast is located in 90° yaw angle. So most probably they make more noise compare to other two cases.

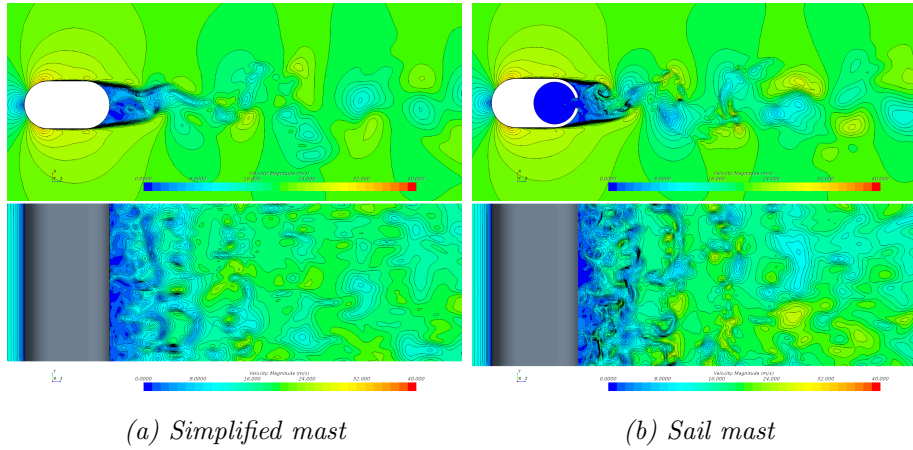


Figure 5.1: Velocity contour plots for $\psi = 0^\circ$ in range of $0 \frac{m}{s}$ to $40 \frac{m}{s}$ shown by plane section at $y = 0$ and $x = 0$

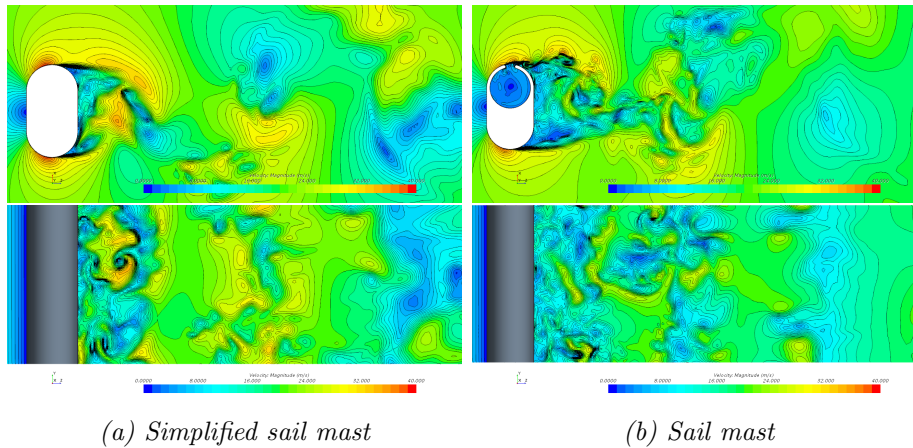


Figure 5.2: Velocity magnitude contour plots for $\psi = 90^\circ$ in range of $0 \frac{m}{s}$ to $40 \frac{m}{s}$ shown by plane section at $y = 0$ and $x = 0$

In Figure 5.3 mean value of velocity magnitude for cases at 0° yaw angle are shown by plane section in $y = 0$ and $x = 0$ which we can see the symmetry shape around the sail mast and simplified sail mast. If the flow is unsteady, the mean velocity usually means time averaged as well. Thus mean value of velocity is important to be plot when we are talking about turbulent flow.

But there was time limitation problem for calculating this scalar value and these cases should be run more to give better figure and completely symmetric shapes.

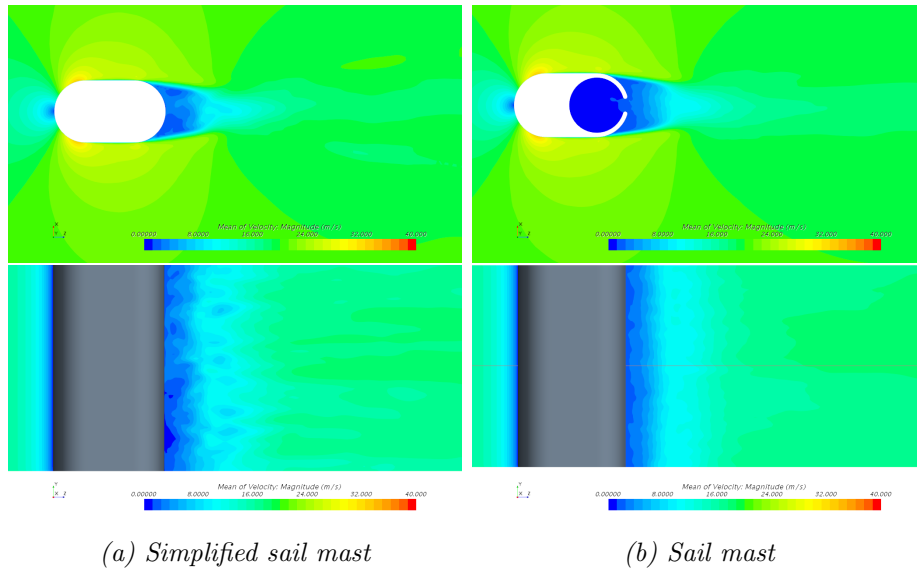


Figure 5.3: Mean velocity magnitude at $\psi = 0^\circ$ in range of $0 \frac{m}{s}$ to $40 \frac{m}{s}$ shown by plane section at $y=0$ and $x=0$

All four cases are represented here and velocity is measured in three different probes around wall of sail mast to find which probe is faced to higher velocity flow. The First case which is simplified sail mast at 0° yaw angle the values are close to each others but the tip probe shows the lowest value and the right probe has the highest value. In the second case which is sail mast in 0° yaw angle, the tip probe is got distance from other two probes and has the lowest power spectral density.

In addition the simplified sail mast which is located in 90° yaw angle shows really close values and it shows there is not a lot of variations in the region of these three probes. last case which is very important case shows that in right and tip probe the velocity magnitude is close in both cases but the right probe is higher one and it can says these two lines are related to existence of vortices near the sail mast tips. It should be take into account that these three probes are located in $y = 0$ which is in the middle of the sail mast in spanwise direction.

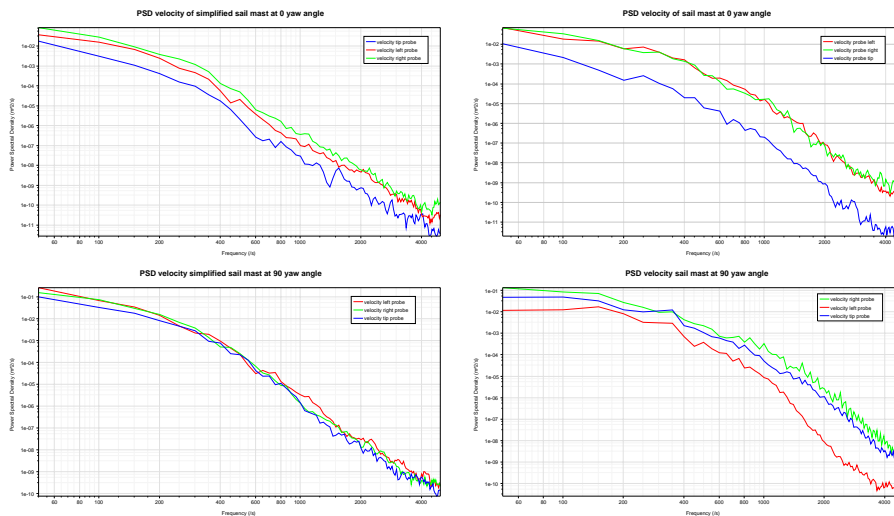


Figure 5.4: Power Spectral Density(PSD) of velocity in all three probes and compare them to each other which is plotted in different frequencies between $0(Hz)$ to $4500(Hz)$

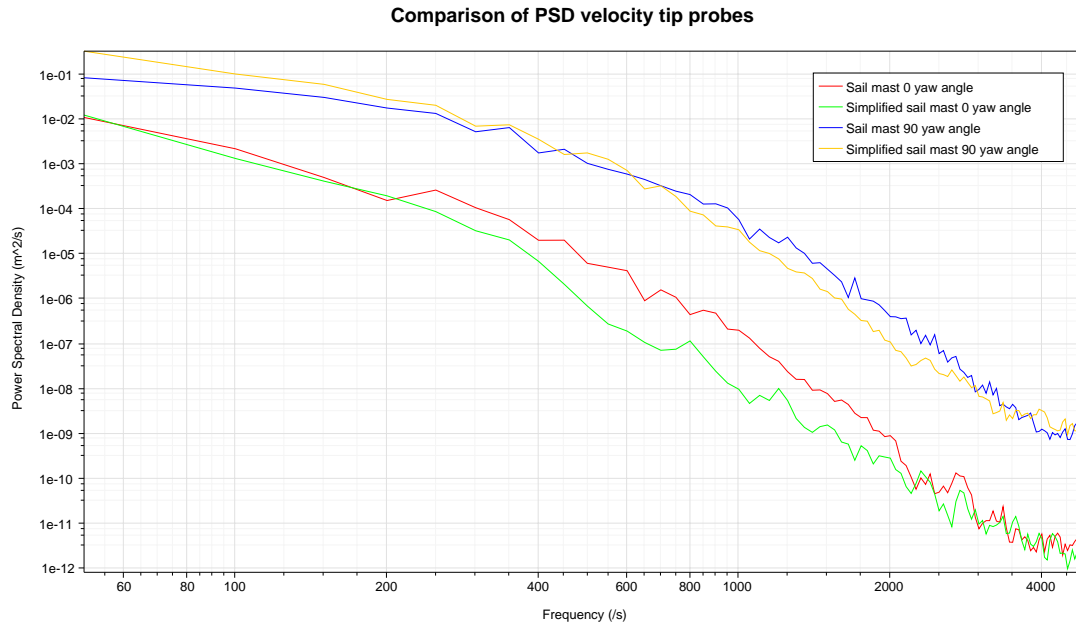


Figure 5.5: Power Spectral Density(PSD) of velocity in tip probes and compare them to each other which is plotted in different frequencies between 0(Hz) to 4500(Hz)

Moreover in Figure 5.5 the tip velocity at the sail mast in 90° yaw angle has the highest value in the graph and it is logical to find out that the probe which is located in downstream of the simplified sail mast in 0° yaw angle is faced to the lowest velocity value. If they are being compared it can be shown that two cases with 90° yaw angle have higher value than the cases with the 0° yaw angle.

5.1.2 Pressure

From Bernoulli equation it is clear that pressure is inversely related to velocity, and it means that high velocity gives low pressure and vice versa. In the following figures, it can be seen high pressure area is located where the flow impacts the sail mast and low pressure area where the flow later accelerates around the sail mast. There are some similarities seen between the cases. As they are shown here all of them have the same point of separation and the shape of the boundary layer is very similar in each yaw angles. Furthermore by looking at case *b* in both yaw angles we observe that in the middle of the sail mast some strong vortices are generated on downstream of the sail mast which identified by low pressure cores. But in the first case vortices generated by shear layer detaching from the curvature and mast's tips do not have a lot of impact like second case because in 90° yaw angle sail mast's tips play the most dominant role to generate the vortices. The highest pressure in each cases can be found in front of case studies due to high velocity that is like pressure distribution around bluff body.

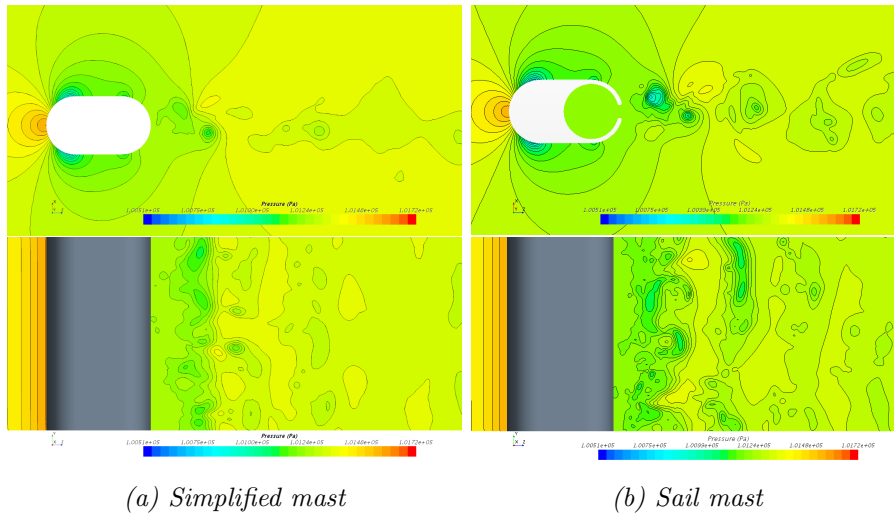


Figure 5.6: Pressure contour plots for $\psi = 0^\circ$ in range of 1.0051×10^5 (Pa) to 1.0172×10^5 (Pa) shown by plane section at $y=0$ and $x=0$

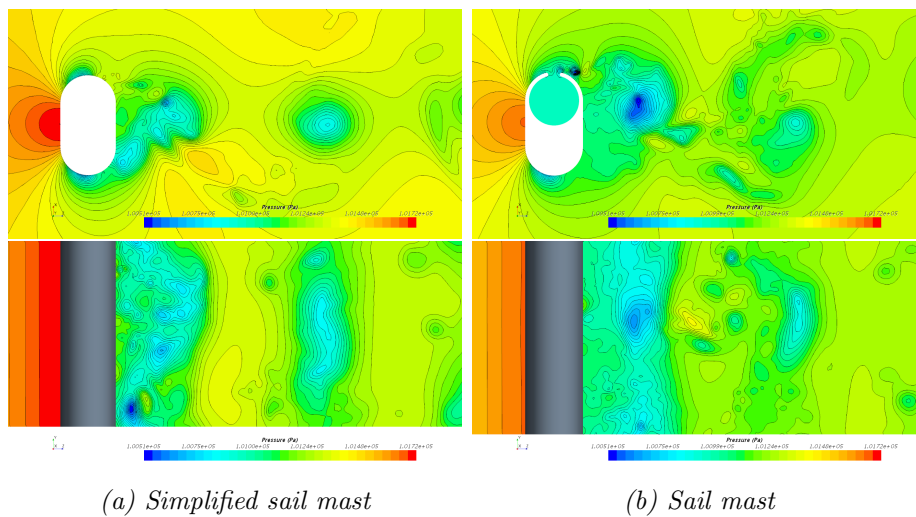


Figure 5.7: Pressure contour plots for $\psi = 90^\circ$ in range of 1.0051×10^5 (Pa) to 1.0172×10^5 (Pa) shown by plane section at $y=0$ and $x=0$

5.1.3 Contour plots of vorticity

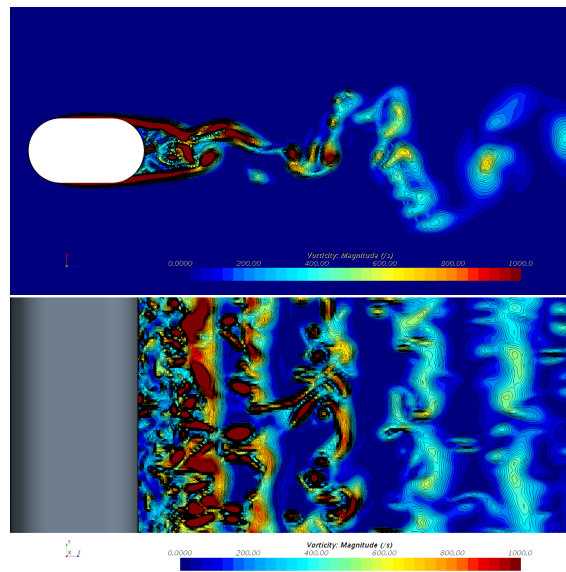
It was important to analyze the vorticity contour plots, as they depict the vortex shedding is correlated to noise generation. As we know existence of vorticity is strongly related to pressure distribution and we have vortex when the flow is rotating around a axis. By looking at the flow structures behind the sail masts, a lot of vortices are shown. In mathematical point of view, vortices can be characterized by three variables vorticity, velocity and circulation. Vorticity can be explained as local rotation of motion at specific location in fluid. So if there is no vorticity the flow is called irrotational. Specially in turbulent flow study vortices are pertinent area of investigation and as it is shown here downstream of the sail masts is full of vortices and they can generate noise at far field area.

$$\omega = \frac{1}{2}(\nabla \times V) = \frac{1}{2} \begin{vmatrix} i & j & k \\ \frac{\partial}{\partial x} & \frac{\partial}{\partial y} & \frac{\partial}{\partial z} \\ u & v & w \end{vmatrix} \quad (5.1)$$

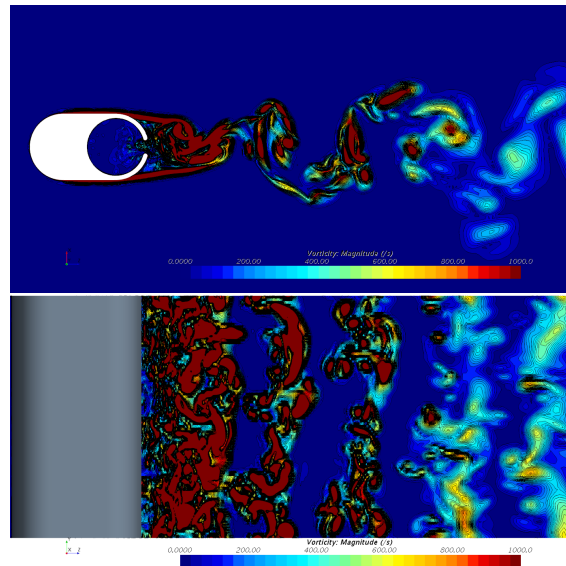
$$\omega_x = \frac{1}{2} \left(\frac{\partial w}{\partial y} - \frac{\partial v}{\partial z} \right), \omega_y = \frac{1}{2} \left(\frac{\partial w}{\partial x} - \frac{\partial u}{\partial z} \right), \omega_z = \frac{1}{2} \left(\frac{\partial v}{\partial x} - \frac{\partial u}{\partial y} \right) \quad (5.2)$$

So it is clear that vorticity is related to variation of velocity. In the following part vorticity contour plots of the four cases are shown and the range of vorticity magnitude is set between 0 to 1000 s^{-1} .

As we can see in Figure 5.11 it shows there is stronger vorticity in sail mast at 90° yaw angle near the tips and one of the indicator that shows we have much more noise in this shape can be existence of vortices.

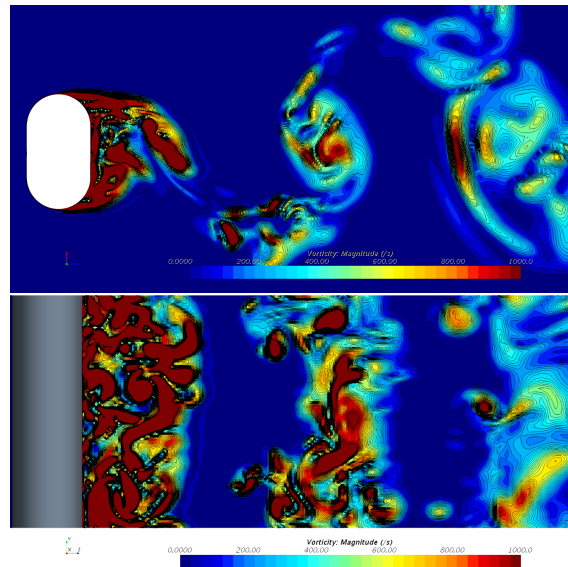


(a) Simplified sail mast

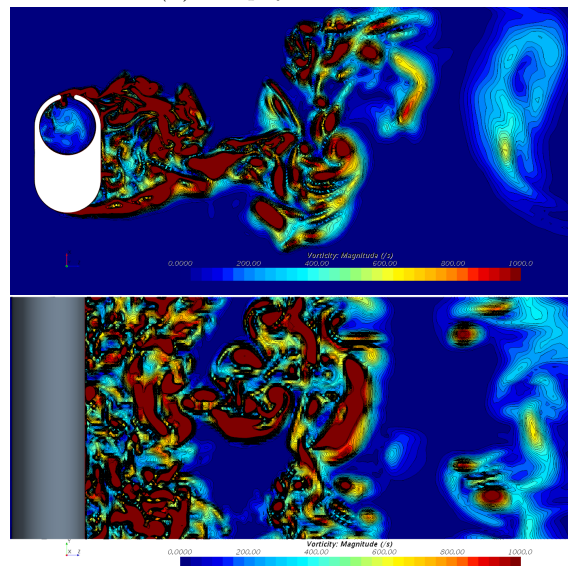


(b) Sail mast

Figure 5.8: Vorticity magnitude contour plots at $\psi = 0^\circ$ in range of 0 s^{-1} to 1000 s^{-1} shown by plane section at $y=0$ and $x=0$



(a) Simplified sail mast



(b) Sail mast

Figure 5.9: Vorticity magnitude contour plots at $\psi = 90^\circ$ in range of $0s^{-1}$ to $1000s^{-1}$ shown by plane section at $y=0$ and $x=0$

Unit of vorticity is the same as frequency so it can be sensible if some probes are located in the downstream part of sail mast to plot the Power Spectral Density(PSD) of static pressure. Here three different probes located near the wall to derive the static pressure. First figure shows comparison of static pressure on tip probes and it can be found that the probe that is located exactly back of the simplified sail mast shows the lowest Power Spectral Density(PSD) and it is logical because if we look at the vorticity plot this phenomena is clear and the vorticity magnitude in this region is lower than others. Further more a peak is found for the sail mast in 90° yaw angle and we can say that whenever we have strong vorticity we have peak at PSD graph. In Figure5.11 all four cases are compared to each other to find the differences of static pressure in tip probes, the sail mast with higher yaw angle has the highest value which there is also a peak around 400(HZ).

The Han window is used as the window function here and in the computation of the PSD in the study, the time samples are divided into ten segments with the same length and 50% overlapping.

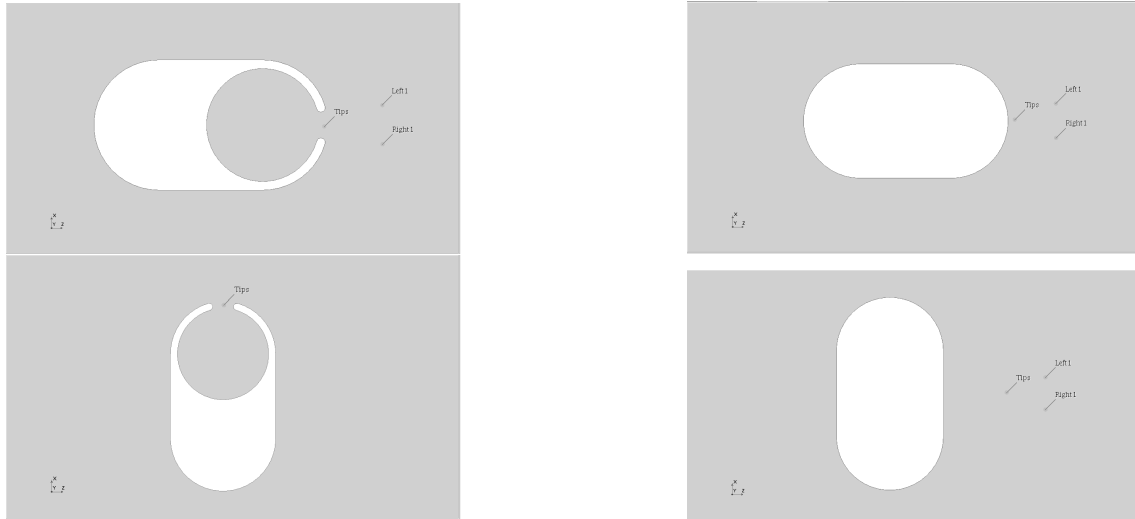


Figure 5.10: Top view of probe's locations around the sail mast and simplified mast to measure pressure and velocity

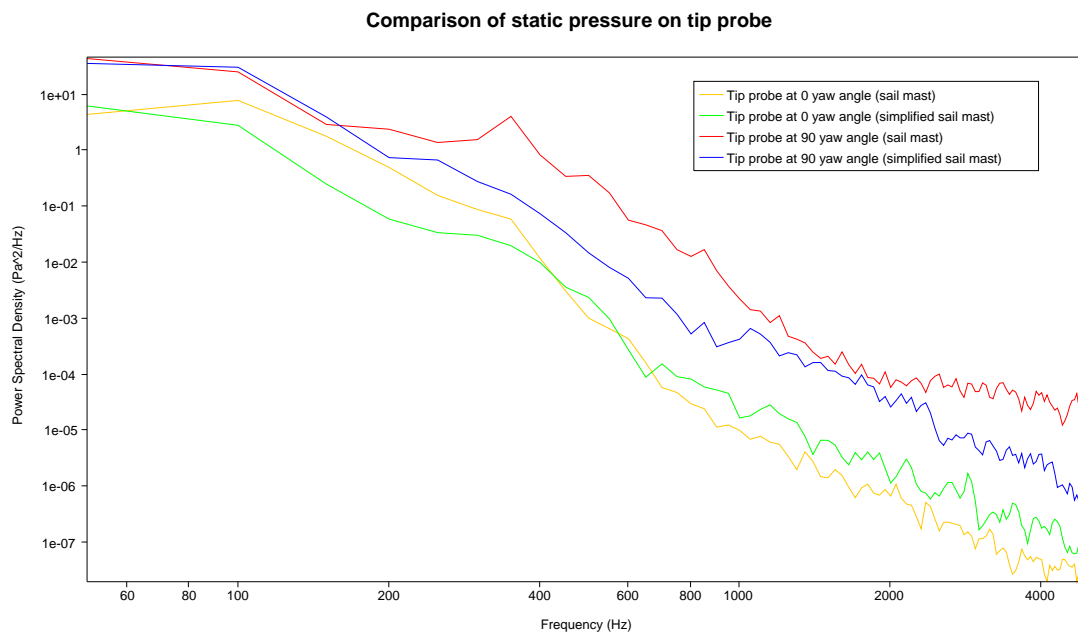


Figure 5.11: Comparison of static pressure on tip probes in among all four cases which is plotted in different frequencies between 0(Hz) to 4500(Hz)

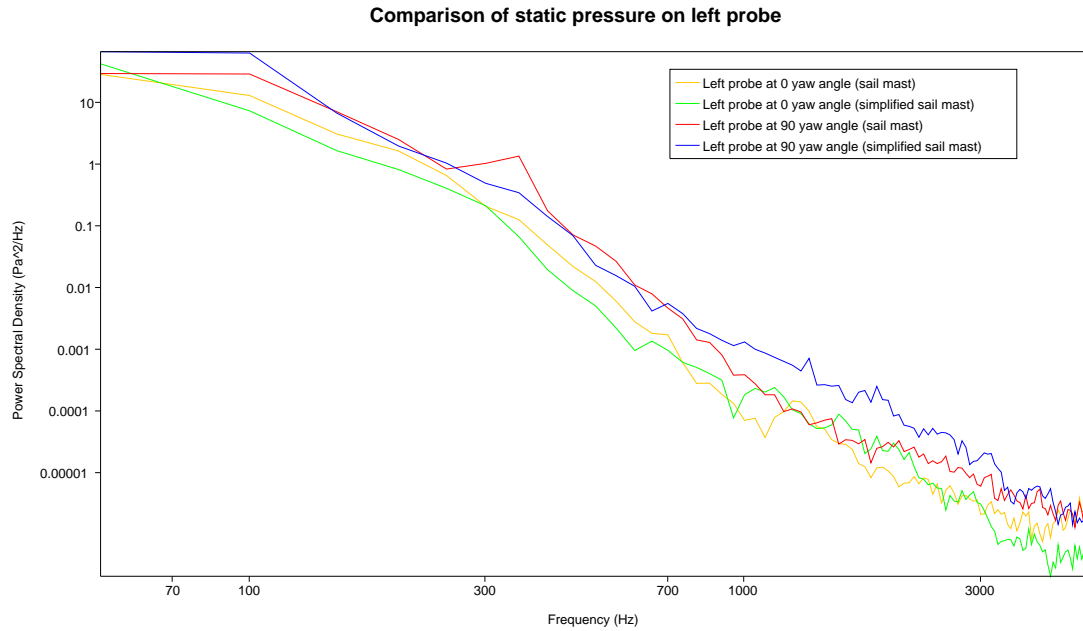


Figure 5.12: Comparison of static pressure on left side probes among all four cases which is plotted in different frequencies between 0(Hz) to 4000(Hz)

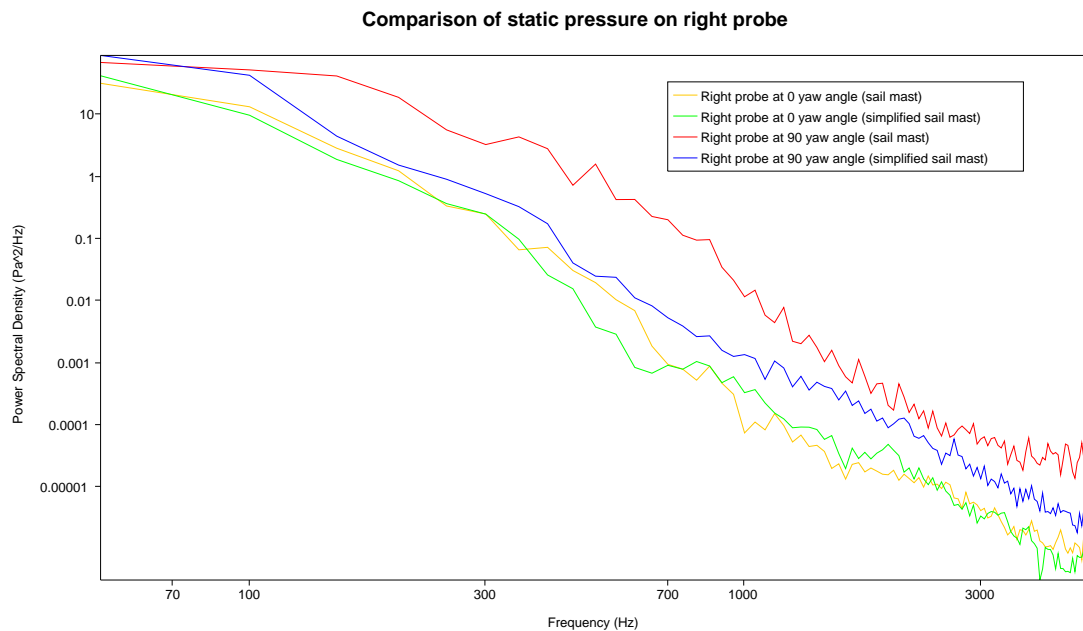


Figure 5.13: Comparison of static pressure on right side probes among all four cases which is plotted in different frequencies between 0(Hz) to 4000(Hz)

5.1.4 Visualization of flow structures

The λ_2 criterion is a technique that was utilized to visualize the vortices in the turbulent flow using isosurfaces and to identify the flow structures downstream of the sail mast this method is used here by showing an isosurface which is a surface in space where λ_2 is constant. From the images we observe how most of the vortical

structures are generated by the separation and recirculation induced by the cavity, and how they evolve, becoming larger and at the same time less intense. And many vortices are seen in downstream of sail mast and mast's tips that can be main noise sources.

Here instantaneous isosurfaces of streamwise vorticity magnitude at $2500s^2$ shaded with streamwise velocity that they are colored by instantaneous pressure and is predicted by DES model. Plus the range is set between $1.009 \times 10^5 pa$ to $1.0157 \times 10^5 pa$. So from these four cases we can find out the flow structures are completely different when the sail mast is located in 90° yaw angle because the flow is faced to large surface and separation is happen earlier than 0° yaw angle. By considering case *b* in Figure 5.8 and Figure 5.9 the region which we have flow is shown and it is clear that the flow goes into to the cavity and changes the flow structure. And the pressure is lower on down stream of the sail mast compare to the simplified shape because of cavity existance. In addition, in simplified cases higher pressure can be seen and it is caused by cavity and the sail mast's tips because when the flow passes the sail mast it goes in to the cavity and it makes changes in flow structure.

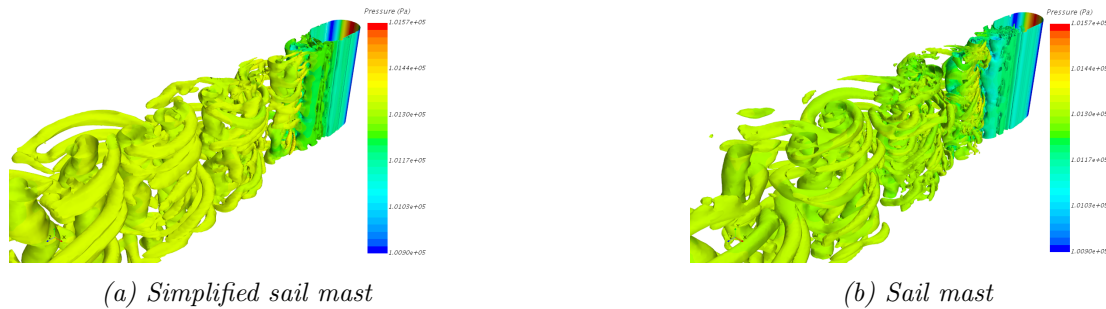


Figure 5.14: Flow structures colored by pressure at $\psi = 0^\circ$



Figure 5.15: Flow structures colored by pressure at $\psi = 90^\circ$

5.1.5 Velocity profile and force coefficients

The following images show the scalar velocity magnitude and pressure along the models on XY plot which uses data that are taken from the line probe which is drawn from inlet to outlet in z direction with smooth values activated. As it was mentioned before the length of the computational domains are 8 meters and the object is located 3 meters far from the inlet and 5 meters from outlet. In the Figure 5.16 the highest pressure is shown for both cases which are located in 0° yaw angle, for case *a* it is around 101550(pa) and case *b* is 101575(pa). Both of the high values

are taken from near the wall. The important variable of next two figures is velocity value which in case *a* it started from inlet by 20m/s and goes to $z = 0.5\text{ m}$ that has 26m/s . The highest velocity among all cases is shown here in case *b* by around 28 m/s in $z = 1.5\text{m}$ along downstream of the sail mast. Furthermore the velocity value changes a lot on downstream of the sail mast at 90° yaw angle and this phenomena is compatible with Section 5.1.4.

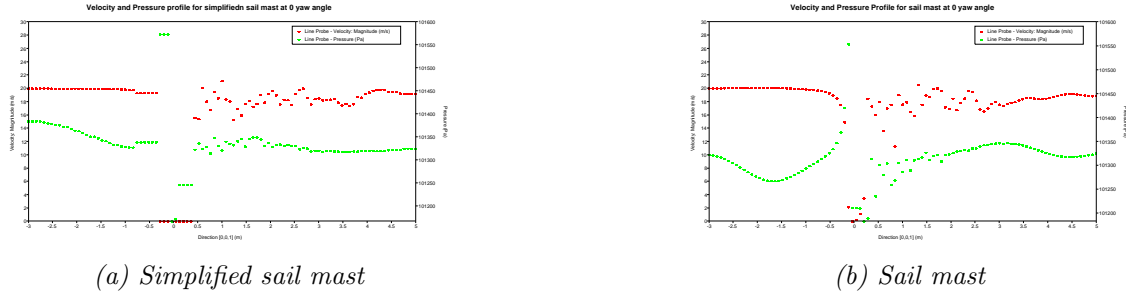


Figure 5.16: Velocity and pressure profiles for $\psi = 0^\circ$ along z direction

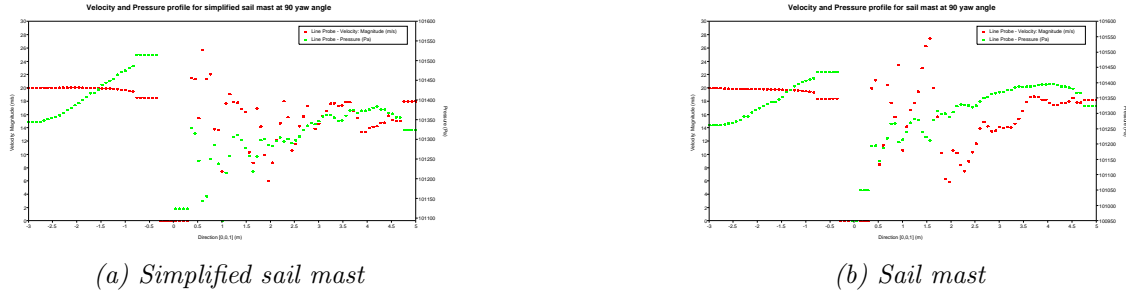


Figure 5.17: Velocity and pressure profiles for $\psi = 90^\circ$ along z direction

Lift coefficient (C_L) and Drag coefficients (C_D) are calculated for all four cases in this part, in all cases $\rho = 1.225 \frac{\text{kg}}{\text{m}^3}$, $V = 20 \frac{\text{m}}{\text{s}}$, $A_{ref} = 0.075\text{m}^2$ and A_{ref} is determined by *spanwiselength* \times *Crosssection length*, $0.5\text{m} \times 0.15\text{m} = 0.075\text{m}^2$. To compare both force coefficients A_{ref} is set to the same number because it gives us better sense to compare forces.

$$C_{Dz} = \frac{D_z}{\frac{1}{2}\rho V^2 A_{ref}} \quad (5.3)$$

$$C_{Lx} = \frac{L_x}{\frac{1}{2}\rho V^2 A_{ref}} \quad (5.4)$$

Cases	$\psi = 0^\circ$	$\psi = 0^\circ$ simplified	$\psi = 90^\circ$	$\psi = 90^\circ$ simplified
C_{Dz}	0.3677	0.2935	2.2888	2.2163
C_{Lx}	0.0729	-0.016	-0.1323	-0.0317

Table 5.1: Drag and lift coefficients

The table 5.1 shows that drag coefficient is really different in $\psi = 90^\circ$ cases and this is logical because we face to larger surface that flow pass and the biggest

drag coefficient is for sail mast in 90° yaw angle and most probably is caused by the cavity because the flow goes in the mast. So highest value is presented by sail mast at $\psi = 90^\circ$ which is 2.2888 and the lowest value is owned by simplified at $\psi = 0^\circ$ that is 0.2935. Moreover When we look at the lift coefficient results in the $\psi = 0^\circ$ yaw angle cases the results are near zero because of symmetry geometries, there is the small differences with zero that could be because of uncertainty. About lift coefficient values we could guess from the start point in symmetric cases that should be near zero. The two cases at $\psi = 0^\circ$ validate this assumption but for the sail mast at $\psi = 90^\circ$ most probably the limitation of simulation time lead to have a value around -0.1323, so it needs to be run more and irregularity in force coefficient can be explained by irregular three dimensional break up of vortices.

5.2 Sound sources

The flow behavior in the cases which have cavity inside may be understood by investigation the result of instantaneous vorticity contours shown in 5.1.3 section. These pictures show the flow behaviour in vicinity of the cavity opening and the behaviour of the unsteady flow which leads to separation of shear layer around the cavity. The shear layer instabilities which distribute small pressure disturbances growth and these instabilities leads to unsteady impingement of the shear layer layer on the back of the cavity. As the result of this behaviour the pressure in the vicinity of the cavity fluctuates in a periodic manner.

In addition it can be seen that in the shear layer space and time changes in a linear way. And the pressure perturbation radiate with sound from the bluff body and flow make more noise by passing through the cavity and the frequency of the disturbance follow the developing shear layer that we can see the results in the following sections. When the flow goes inside the cavity circulation process is started and in the following when it tries to go out from the cavity this process leads to small scale vortex shedding which is completely shown in 5.1.2 section. So from now we can focus on vortex that are made by the bluff body and sail mast tips and investigate how it generate sound.



(a) Simplified sail mast

(b) Sail mast

Figure 5.18: Comparison of flow structure affected by cavity and bluff body on down stream colored by pressure in range of 1.009×10^5 and 1.0157×10^5 , case studies at $\psi = 0^\circ$



(a) Simplified sail mast

(b) Sail mast

Figure 5.19: Comparison of flow structure affected by cavity and bluff body on down stream colored by pressure in range of 1.009×10^5 and 1.0157×10^5 , case studies at $\psi = 90^\circ$

Vortex sound is the sound generated by unsteady fluid motions. The sound production in subsonic flows is related to the dynamics of vortices which are made by case studies. Comparison between vorticity $\omega = \nabla \times v$ and Reynolds stress shows that there is a large region of potential flow that does not produce noise. As it is known at low Mach number free field conditions are applied and vortex sound can be predicted better because there is no sound reflections and the receivers can receive the direct sound from the noise sources.

Moreover we know velocity field can be divided into a potential and a vortical part. The potential part of the flow is strongly related to dilatation rate of fluid particles. We know the acoustical flow is basically compressible and unsteady. So if acoustic part be consider as the unsteady component of the potential flow we can present it like here:

$$u_{ac} = \nabla \phi' \quad (5.5)$$

Right hand side of this equation shows the time dependency of potential flow and left side is the unsteady component of the potential flow. The equation of Euler here is in the form of :

$$\frac{\partial v}{\partial t} + \nabla B = \frac{f_c}{\rho} \quad (5.6)$$

Sound vorticity of the flow is defined on righth hand side of the equation. And in low Mach number variation of the density can be neglected and at the end f_c is the source of sound.

The power generated by the vortices in the flow can be written in the form of:

$$\langle P \rangle = \int \langle f_c \cdot u_{ac} \rangle dV \quad (5.7)$$

The left side is the time averaged acoustical power which are generated by the vortices of the flow . As some contours plots of vorticity are shown above it is clear that the amount of vortices which are gotten from four cases are different from each other and these vortices are linked to sound generations that we are looking for. Next section is going to talk about pressure fluctuation which we can get by the receivers far from the sound sources to show how much noise each case make and compare all these four models together.

5.2.1 Far-field noise

In aero-acoustics, there are several methods to measure sound source. The method used here, is Ffowcs Williams and Hawkins(FWH) which is based on Lighthill's acoustic analogy.

Figure 5.20 shows the resolved and synthesized noise components at 36 receivers which are located around the computational domain and the respective Fourier transforms of all four models are shown in terms of sound-pressure levels (SPL) in the following figures. The composite signal shows the closest agreement with data and discrete nature of the energy distribution in the synthetic reconstruction model is evident in the higher-frequency components.[20] Also harmonic shape of oscillation can be observed in both cases after a while when the simulation is run enough. Moreover oscillation of the case study in 90° yaw angle is much more than what is seen at 0° yaw angle and first period of each case has high oscillation.

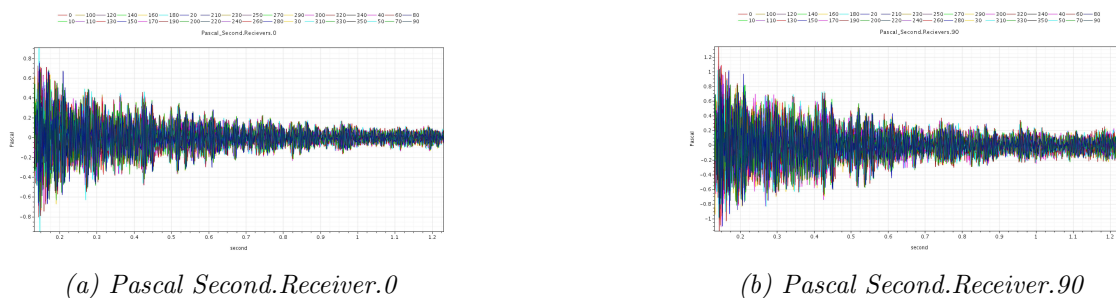


Figure 5.20: Pascal Second graph of all 36 Receivers located around computational domain

The farfield characteristics of the generated sound field are investigated by using the Ffowcs Williams-Hawkings integral equation. The size and position of integral surface are very important and they have a lot of impact on the accuracy of the numerical predictions. So in our case this surface is located around the case studies and it continued to output of the computational domain to estimates accurate sound pressure levels. Another important issue which can have influence on the results is the length of the integration surface in the streamline direction and this dimensions are found by experiments and limited by the size of computational domain. So the farfield generated noise is evaluated by calculating the pressure signals at 36 receivers which are located on radius of 10m around the computational domain and they show difference of all case studies in generating noise.

As it was mentioned above noise and vorticity does in theory have a strong correlation. So to investigate noise generation the Sound Pressure Level (SPL) of the pressure fluctuations at 36 receivers are plotted but here only some of them are shown 0° , 90° , 180° and 270° . The pressure fluctuations at the figures are made by

turbulent flow structures and we can say they are characteristics frequencies of the shear layers. In addition a dominant peak which is shown in sail mast with $\psi = 90^\circ$ yaw angle comes from the high energy that is generated by the model. And higher sound pressure level coincides with a higher degree of vorticity around the models. The goal of the project is to investigate and find if there is any tonal noise and what are the tonal noise sources which originate from the impulsive noise. If we take a look at the Sound pressure level(SPL) figures we can compare the level of noise generation among these four cases. Moreover we can see from graphs that simplified sail mast on $\psi = 0$ makes the lowest noise compare to others because sound pressure level goes to zero before 3000(Hz) which this phenomena happen later and in higher frequencies for three other cases. Moreover the noise generation which we see in the sail mast at $\psi = 0$ is the result of having cavity inside the sail mast which make this graph similar to simplified sail mast at $\psi = 90$ both of them generate similar noise in general view. This explanation can lead to better view for analyzing the last case which is sail mast at $\psi = 90$. We can indicate that sound pressure level in all receivers are continued after 3000(Hz) and slightly after 300(Hz) at approximately 320(Hz) we have sharply increase. Since the peak which has high energy in the figure is located within 300–330Hz, which ranges a narrow frequency bandwidth We can regard the peak as the tonal noise. Comparison among all receivers in four cases shows symmetric locations of 90° receiver and 270° receiver make their data similar to each other, green and yellow line are completely close to each other. In addition in each SPL figure 0° receiver mostly has higher value and the receiver at 180° has the lowest value as we could guess before 0° receiver is located exactly back of the model and 180° is in front of the study cases. This issue says the turbulence in the wake region plays a dominant role in noise generation.

By looking at first two cases it can be found the range of noise generation dose not pass 3000(HZ) in first case which is simplified sail mast and in other hand second case goes to near 4000(HZ) and also higher sound pressure level can be seen in the second case . To compare third and forth cases it can be discover that the last case is generating more noise and there is a dominant peak around 400(HZ) which can be produce tonal noise. By these four figures it is possible to analyze the flow structure and the resulting acoustic wave propagation. Here Several basic features can be found by associated with noise emission related to specific frequencies in the pressure spectra. The frequency spectrum observed at the recievers in 90° and 270° are extremely similar to each other because of flow structure symmetry. An important part of pressure spectrum of turbulent flow is mostly related to the flow which is shaded and the impact of cavity to make the wake region on downstream of the cases. Two different phenomena occur here: mixing layer and vortex shadding that make the dominant part of Sound Pressure Level (SPL) figures.

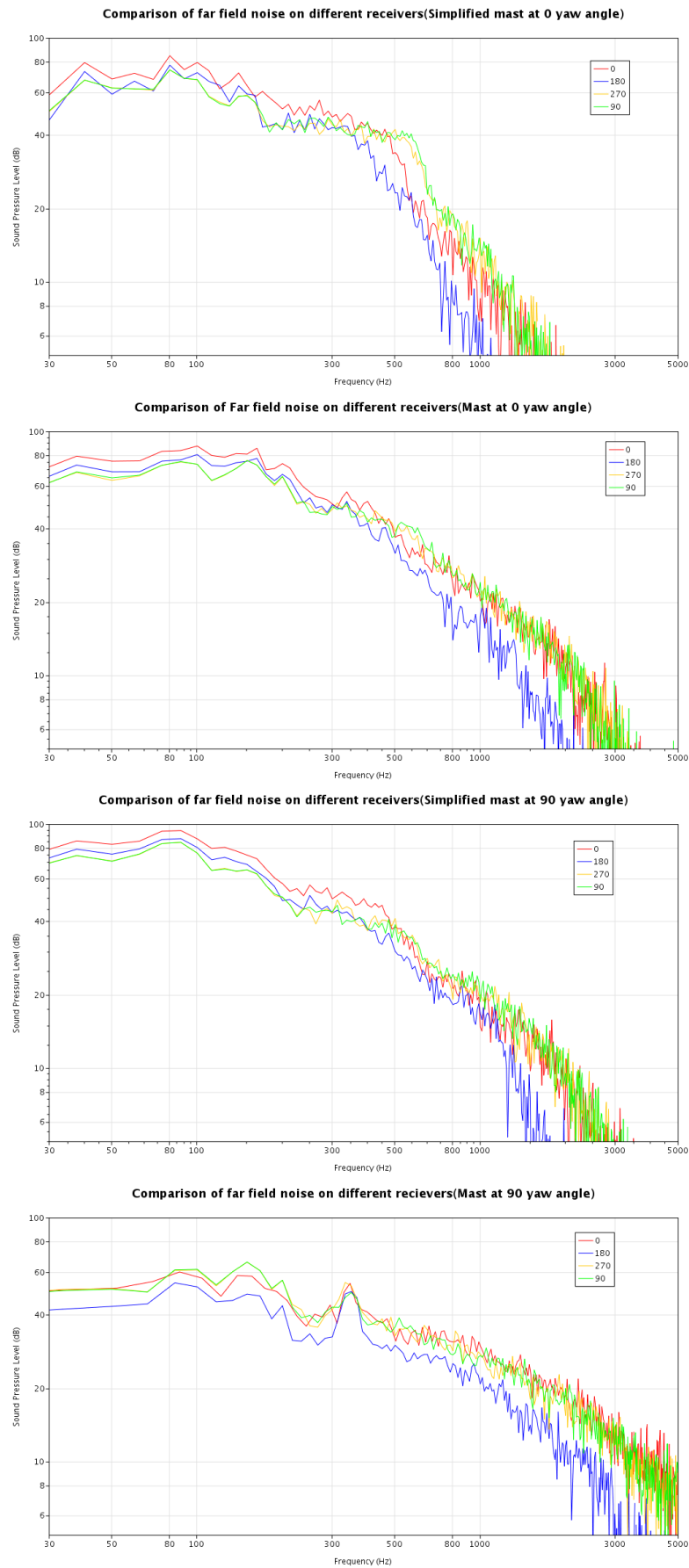


Figure 5.21: Comparison of Sound Pressure Level(SPL) graph in all four cases which are changed by different frequencies between 30(Hz) to 5000(Hz)

Chapter 6

Conclusion

6.1 Final discussion

To talk about general results it is found that sail mast at 90° yaw angle generates higher noise compare to other cases this is what i was expected from first point of the project. Tonal noise has not been recorded during the simulations of three cases and only the case which is the sail mast at 90° shows peak at Sound Pressure Level figure that could be tonal noise. In other hand from the three cases that were mentioned above only broadband noise was captured. A topic of interest is yaw angle which was done for 0° and 90° . As it was shown in result parts the vorticity does not reach to the sail mast tips in 0° yaw angle . In another case, the vorticity was observed near the tips and this phenomenon could be the reason to get much more noise from this case.

In chapter 5 more noise was shown which is created by the sail mast when there is high level of vorticity around the tips. By looking at section 5.1.3 it is possible to notice that there is vorticity around the tips in sail case at 90° yaw angle and in another case which is located in 0° yaw angle there is no vorticity near the tips this can be dominant difference because the aim of the project could be investigating of the sail mast tips to find noise sources. Furthermore when the wake region is considered to be analyzed in section 5.1.3 we can see the cavity inside the sail mast can be cause of creating vorticity in wake region because as we could guess the flow goes into cavity and make disturbances around the sail mast. The cavity space inside a sail mast has its own effect for example if sail can be folded into the mast it fill out the space inside the sail mast and a full cavity can make less noise.

A source of error could be that in real life the flow is always turbulence and there is fluctuations in the wind. It can be mentioned separation phenomenon in turbulent flow can create vortices closer to the sail mast tips and the tips could help to make larger pressure fluctuations and noise. Hence the tips of the mast can be the main source of noise generation. Furthermore if the number of cells increase the results most probably could be better but because of lack of time only 3.5 million cells are generated for simplified sail mast and 7.5 millions for the sail mat. The mesh in all cases is performed in similar method and the only difference is to have different number of cells in these cases. As it was mentioned in theory part the coarse mesh can not give us very good result so to make the results good enough the mesh was made fine enough to get noise around the objects. Most probably by finer mesh ,our error to solve the flow near the sail mast can be lower.

Since numerical computations have been used in the project there was possibility to have some errors in the simulation set up as well. During the project a lot of time was spent for aero-acoustics studies and large resources were needed to run and unsteady 3D computations which was time consuming. Plus valuable time was spent for simulation, post processing and mesh generation part. This was mainly due to difficulties when setting up the physics for capturing the aero-acoustic features and various boundary conditions and properties were therefore tested in order to acquire a converged solution.

Here only 0.5 m of the sail mast is considered and if the whole sail mast would be considered the result can be different and the mesh has also strong effect in numerical analysis. In addition if these cases are faced to different yaw angles most probably the results are not the same as this project. So different yaw angle and diameters can be study to compare the results. It is possible to find out whistling noise in other yaw angles can be made by the tips. As in the theory part was mentioned whistling can most probably occur due to vortex shedding which comes from tip's shape. This field is really interesting for researchers because there is strong connection between aerodynamic and acoustic science which a lot of high technology company are making plan to do research on this field to reduce noise of their product.

6.2 Future work

To sum up the result and talk about future plans we can add that the project goal was analyzing effect of sail mast's tips in sail mast noise generation and looking for the tonal noise in all four cases. It was concluded that only the case which is sail mast located at 90° yaw angle makes tonal noise in sound pressure level (SPL) figure. In another side of the project other three cases only generate broadband noise. It is very important to keep in mind that these results are not fully verified but from the past projects these results can be trusted and the sail mast with 90° yaw angle generate more noise than others.

This study concludes that sail mast at 90° can make tonal noise and if want to avoid this phenomenon changing geometry of sail mast tips and curvature of them most probably leads to have this chance to decrease the noise generation and different yaw angles with different velocity can be studied to validate final result of the project and in experimental point of view there is some solution to postpone the separation points. It must be clarified that the experimental acoustic data for these configurations are not available yet. Thus experimental work should be done to compare with numerical analysis and provide a complete result about aerodynamic and aeroacoustic of sail mast.

Appendix A

Appendix

A.1 Streamline

A streamline is defined as a line which is parallel to the local velocity and several streamlines together form a flow pattern which they are colored by velocity in stream wise direction and we can find that in some part the velocity direction is negative it means the flow goes back and these parts are shown by blue color. The range of velocity is set between -35 to 35 m/s .



Figure A.1: Streamline colored by velocity in streamwise direction at $\psi = 0^\circ$



Figure A.2: Streamline colored by velocity in stream wise direction at $\psi = 90^\circ$

A.2 Variance

Variance: the field variance is the sample variance of a field function value as the solution progresses each cell or boundary face in the selected parts. The statistical variance is based on data samples collected at a user specified frequency for each parts being monitored.

$$s^2(x) = \frac{1}{N-1} \left[\sum_{i=1}^N x_i^2 - \frac{1}{N} \left(\sum_{i=1}^N x_i \right)^2 \right] \quad (\text{A.1})$$

A.3 Overall sound pressure level

In order to visualize the direction in which the highest level of noise is produced, the Overall Sound Pressure Level was computed in every receiver location. The OASPL is based on the root mean square value of the pressure fluctuations.

Bibliography

- [1] S CD-adapco. “STAR CCM+ User Guide Version 12.04”. In: *CD-Adapco: New York, NY, USA* (2017).
- [2] Fabien Anselmet and Pierre-Olivier Mattei. *Acoustics, aeroacoustics and vibrations*. John Wiley & Sons, 2016.
- [3] GB Ashcroft, K Takeda, and X Zhang. “A numerical investigation of the noise radiated by a turbulent flow over a cavity”. In: *Journal of Sound and Vibration* 265.1 (2003), pp. 43–60.
- [4] RS Cant. “SB Pope, Turbulent Flows, Cambridge University Press, Cambridge, UK”. In: *Combustion and Flame* 125 (2001), pp. 1361–1362.
- [5] Shiyi Chen et al. “Reynolds-stress-constrained large-eddy simulation of wall-bounded turbulent flows”. In: *Journal of Fluid Mechanics* 703 (2012), pp. 1–28.
- [6] Lars Davidson. *Fluid mechanics, turbulent flow and turbulence modeling*. 2015.
- [7] Ing Jan Delfs. “Basics of Aeroacoustics”. In: *Technical University of Braunschweig, Braunschweig* (2014).
- [8] Joel H Ferziger and Milovan Peric. *Computational methods for fluid dynamics*. Springer Science & Business Media, 2012.
- [9] Mike Goldsmith. *Discord: The story of noise*. Oxford University Press, 2012.
- [10] Sebastian Grashorn and Emil V Stanev. “Kármán vortex and turbulent wake generation by wind park piles”. In: *Ocean Dynamics* 66.12 (2016), pp. 1543–1557.
- [11] Karl E Gustafson and James A Sethian. *Vortex methods and vortex motion*. Vol. 19. SIAM, 1991.
- [12] Colin H Hansen. “Fundamentals of acoustics”. In: *Occupational Exposure to Noise: Evaluation, Prevention and Control. World Health Organization* (2001), pp. 23–52.
- [13] Michael S Howe. *Theory of vortex sound*. Vol. 33. Cambridge University Press, 2003.
- [14] Michael Charles Irwin. *Smooth dynamical systems*. Vol. 17. World Scientific, 2001.
- [15] Anastasios S Lyrintzis. “Surface integral methods in computational aeroacoustics—From the (CFD) near-field to the (Acoustic) far-field”. In: *International journal of aeroacoustics* 2.2 (2003), pp. 95–128.

- [16] Milovan Peric and Stephen Ferguson. “The advantage of polyhedral meshes”. In: *Dynamics* 24 (2005), p. 45.
- [17] Alan Powell. “Why do vortices generate sound?” In: *Journal of Mechanical Design* 117.B (1995), pp. 252–260.
- [18] Sjoerd W Rienstra and Avraham Hirschberg. “An introduction to acoustics”. In: *Eindhoven University of Technology* 18 (2003), p. 19.
- [19] Matic Šavli. “Turbulence kinetic energy–TKE”. In: *University of Ljubljana, Faculty of Mathematics and Physics, Department of Meteorology. Seminar: 4th Class. May*. Vol. 27. 2012.
- [20] Claus Wagner, Thomas Hüttl, and Pierre Sagaut. *Large-eddy simulation for acoustics*. Vol. 20. Cambridge University Press, 2007.
- [21] David C Wilcox et al. *Turbulence modeling for CFD*. Vol. 2. DCW industries La Canada, CA, 1998.
- [22] Hua-Dong Yao and Lars Davidson. “Generation of interior cavity noise due to window vibration excited by turbulent flows past a generic side-view mirror”. In: *Physics of Fluids* 30.3 (2018), p. 036104.
- [23] Hua-Dong Yao, Lars Davidson, and Lars-Erik Eriksson. “Noise radiated by low-Reynolds number flows past a hemisphere at $Ma=0.3$ ”. In: *Physics of Fluids* 29.7 (2017), p. 076102.
- [24] Hua-Dong Yao et al. “Surface integral analogy approaches for predicting noise from 3D high-lift low-noise wings”. In: *Acta Mechanica Sinica* 30.3 (2014), pp. 326–338.
- [25] Huadong Yao, Zenitha Chroner, and Lars Davidson. *Simplifications Applied to Simulation of Turbulence Induced by a Side View Mirror of a Full-Scale Truck Using DES*. Tech. rep. SAE Technical Paper, 2018.
- [26] Huadong Yao, Lars Davidson, and Zenitha Chroner. *Investigation of Interior Noise from Generic Side-View Mirror Using Incompressible and Compressible Solvers of DES and LES*. Tech. rep. SAE Technical Paper, 2018.
- [27] Oleksandr Zaporozhets, Vadim Tokarev, and Keith Attenborough. *Aircraft Noise: Assessment, prediction and control*. CRC Press, 2011.